



# Mechanical Properties of Limestone After High-Temperature Treatment Under Triaxial Cyclic Loading and Unloading Conditions

Qing-bin Meng<sup>1</sup> · Jiang-Feng Liu<sup>1</sup> · Hai Pu<sup>1</sup> · Li-yuan Yu<sup>1</sup> · Jiang-yu Wu<sup>1</sup> · Cong-kai Wang<sup>1</sup>

Received: 16 December 2020 / Accepted: 27 August 2021 / Published online: 6 September 2021  
© The Author(s), under exclusive licence to Springer-Verlag GmbH Austria, part of Springer Nature 2021

## Abstract

High temperatures can cause deterioration of the physical–mechanical properties of rocks. In this study, the triaxial cyclic loading and unloading of rock specimens under different temperature conditions were investigated to reveal stress–strain curves, strength and deformation characteristics, failure forms, and peak stress dropping of the rock specimens at high temperatures. The deformation of treated rocks has an elastic after-effect, and the stress–strain curves formed a hysteresis loop. Under increasing confining pressures and temperatures, the increase in plastic deformation exacerbated the degree of damage in the rock specimens, and the stress–strain curves gradually transformed from brittle to ductile failure, thereby reducing its severity. With the rise of  $\sigma_3$ , the bearing capacity, strength and deformation of the rock specimens increased, showing an enhancement effect of the confining pressure. With the rise of  $T$ , the effect of deterioration due to temperature was apparent. The brittleness index ( $B_s$ ) of the stress rock specimens was established to quantitatively express the rules of influence from  $\sigma_3$  and  $T$  on the state of post-peak stress drop. Specifically,  $B_s$  increased with the rise of  $\sigma_3$ , whilst the post-peak stress drop ( $N_s$ ) decreased, then increased with the rise of  $T$ . These findings provide a theoretical basis for the analysis of surrounding rock stability, restoration and reinforcement, and the shoring design of underground works following exposure to high temperature such as those occurring after a fire.

**Keywords** High-temperature rock mechanics · Triaxial cyclic loading and unloading · Brittleness index · Strength and deformation parameters

## 1 Introduction

In the course of developing geothermal resources, studies on the underground storage of highly radioactive nuclear waste, the utilization of deep underground space, the prevention of coal/gas explosion in coal mines, and the reconstruction of rock tunnels/mines after a fire are required to understand changes in the physical–mechanical properties of rocks after experiencing high-temperature treatment. This can provide a basis for the design, construction, and support of rock works. The physical–mechanical properties of rocks under high-temperature conditions are strikingly different from those

stored in room temperature conditions. The deformation and mechanical parameters of rocks after high-temperature treatment can provide fundamental data that is indispensable for the analysis of surrounding rock stability, restoration, and the reinforcement and shoring design of underground works. Studies on the mechanical characteristics of rocks after high-temperature exposure and the mechanism of deformation and failure have emerged as a hot topic study of deep rock mechanics (Dwivedi et al. 2008; Heap et al. 2009; Mahanta et al. 2016; Shkuratnik et al. 2019; Shen et al. 2020).

To date, a number of studies have documented the physical and mechanical properties of rocks and their deformation and failure mechanism high-temperatures (Molen 1981; Al-Shayea et al. 2000; Funatsu et al. 2004; Just and Kontny 2012; Tian et al. 2012; Sun et al. 2015; Sha et al. 2020; Li et al. 2020a). Cyclic loading and unloading assays can separate the elastic and plastic strain of loading rock samples, and can be used to quantitatively evaluate the degree of damage at various stages. This represents an effective stress path for studies the laws of rock damage evolution

✉ Jiang-Feng Liu  
jeafliu@hotmail.com

✉ Li-yuan Yu  
yuliyuan@cumt.edu.cn

<sup>1</sup> State Key Laboratory for Geomechanics and Deep Underground Engineering, China University of Mining and Technology, Xuzhou 221116, China

(Rao and Ramana 1992; Fuenkajorn and Phueakphum 2010; Zhao et al. 2013; Li et al. 2018; Pei et al. 2019; Xiao et al. 2020a). Ray et al. (1999) performed cyclic loading tests of sandstone and showed that the strength of the rock sample decreases with the increasing number of cycles. Zhang et al. (2013) performed triaxial cyclic loading and unloading tests on mudstone, and analyzed the influence of plastic deformation on the inelastic deformation characteristics, revealing changes in the laws of the elastic modulus and Poisson's ratio with the cumulative plastic strain. Chen et al. (2016) performed triaxial cyclic loading and unloading tests of rock salt, which analyzed the influence of confining pressure on the shape and elastic modulus of the stress–strain curve. In addition, based on the theory of elastoplastic damage mechanics, the damage evolution law of rock samples during the cyclic loading and unloading process was described. Liu et al. (2016) proposed a new damage constitutive model through the introduction of energy dissipation damage variables based on the results of uniaxial cyclic loading tests. Wang et al. (2017) revealed the evolution of sandstone porosity and permeability under loading and unloading using rock permeability and porosity measurement systems. Yang and Hu (2018) performed long-term creep and permeability tests of rock samples after high temperature (25–1000 °C) under triaxial cyclic loading, and analyzed the relationship between the elastic strain, plastic strain, permeability, temperature and deviator stress. Simultaneously, the evolution law of the creep strain with deviator stress and temperature were revealed. Wang et al. (2019) used the modified split Hopkinson pressure bar system to investigate the cyclic impact of 800 °C temperatures, revealing the strength and deformation evolution laws and deformation failure modes of the rock samples. Based on the maximum strain, an equation describing the damage evolution of rock after high temperature under cyclic impact loading was established. Xiao et al. (2020b) used the true triaxial test system to perform triaxial loading and unloading tests, and studied the influence of loading and unloading pathways on the strength and deformation characteristics, energy conversion and failure modes. They further analyzed the evolution of parameters including the elastic modulus and energy storage capacity with the cycle index. Meng et al. (2016, 2021) performed uniaxial and triaxial cyclic loading and unloading tests, which revealed the evolution of the elastic modulus under different loading rates, and analyzed the evolution of the generalized cohesion, generalized internal friction angle, and dilatancy angle with confining pressure and the equivalent plastic strain. In addition, pre- and post-peak dilatancy models that considered the influence of the confining pressure and the equivalent plastic strain on the volume expansion of the rock samples were constructed.

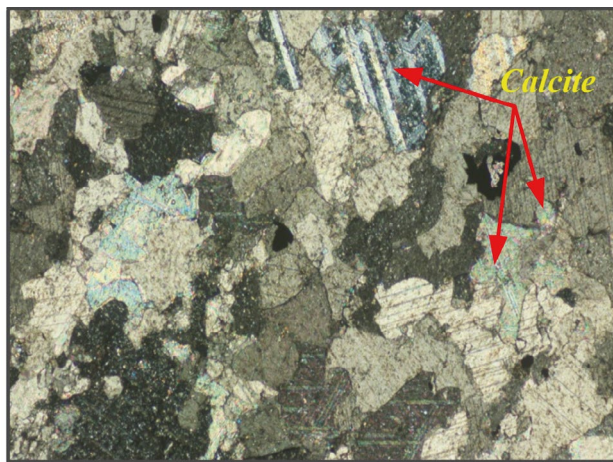
Temperature is an important factor influencing the properties of rocks. Significant changes occur to the physical and

mechanical properties of rocks following exposure to high-temperature treatments. Uniaxial and triaxial compression tests on the physical properties of high-temperature rocks have been performed and have deepened understanding of the physical properties, strength and deformation failure forms of high-temperature rocks. However, most studies to-date have focused on the strength and deformation characteristics of high-temperature rocks under uniaxial and triaxial compression conditions. Studies on the strength and deformation characteristics, volume deformation and post-peak stress drops of high-temperature rocks under triaxial cyclic loading and unloading conditions are limited. Rock is defined as any naturally occurring solid mass or aggregate of minerals or debris formed by a certain law under geological processes. Different rocks possess variable mineral components, structures and formations. The existence of mineral components in rocks and changes to their nature, structure or formation impact their physical and mechanical properties. The mechanical properties of rocks are closely associated with stress conditions, temperature, water and other factors. During the course of rock formation, different temperature effects will occur due to differences in the formation conditions, mineral components and cementing substances, in addition to differences in the geological processes experienced by rocks at later stages. Additionally, rocks of the same type show differences in their temperature characteristics under different geological conditions, exhibiting differences in mechanical behavior under different stress pathways. In this study, limestone exposed to high-temperature treatment was studied and triaxial cyclic loading and unloading tests of rock specimens exposed to 5 different temperatures were performed through the MTS 815 rock mechanics test system. The aim of this study was to define the strength, deformation and dilatancy characteristics of the rock specimens under triaxial loading and unloading conditions, and to deepen understanding of the strength deterioration processes and damage mechanisms of rocks exposed to high-temperature treatment.

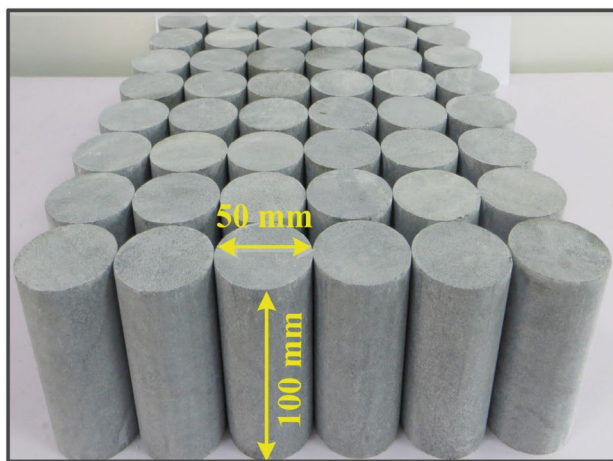
## 2 Testing Equipment and Program

### 2.1 Specimen Preparation and Testing System

Limestone was selected for testing due to its uniform texture, which mainly consists of calcite, dolomite, and illite (Fig. 1a). Types of equipment including the coring machine, sawing machine and grinding machine, were used to process the rock specimens into cylinders with a diameter of 50 mm and a height of 100 mm (Fig. 1b). A GWD-02A high-temperature furnace was used for the high-temperature treatment of rock specimens (Fig. 2a), by setting the temperature ( $T$ ) at five types, viz. 20 °C (room temperature, not heated),



(a) Limestone composition



(b) Rock sample size

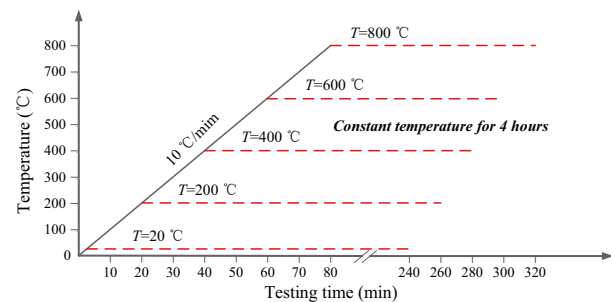
Fig. 1 Limestone composition and sample size

200 °C, 400 °C, 600 °C and 800 °C. The heating treatment design curve of the rock specimens is shown in Fig. 2b. Steps: ① prior to heating, the temperature ( $T$ ) value was set at a rising speed of 10 °C/min (Sun et al. 2015; Su et al. 2017; Meng et al. 2020a; Xiao et al. 2020b). ② When the temperature reached the set value, it was maintained for 4 h to ensure uniform heating inside the specimen, to minimize the negative influence of testing due to non-uniform heating (Heap et al. 2009; Ranjith et al. 2012; Su et al. 2017; Meng et al. 2020a). ③ The furnace was turned off after reaching a constant temperature and allowed to naturally cool to room temperature. The rock specimen was then removed.

Triaxial cyclic loading and unloading tests were performed using the MTS 815 rock mechanics test system (Fig. 3) formed by three parts—loading, testing, and control. The testing machine had a rigidity of  $2.6 \times 10^9$  N/m, an axial load of 1459 kN, a servo valve sensitivity of 290 Hz, and a minimum sampling time of 50  $\mu$ s (Meng et al. 2018,



(a) High-temperature treatment equipment



(b) Thermal treatment design path for rock specimen

Fig. 2 High-temperature treatment and thermal treatment design pathways for the rock specimens

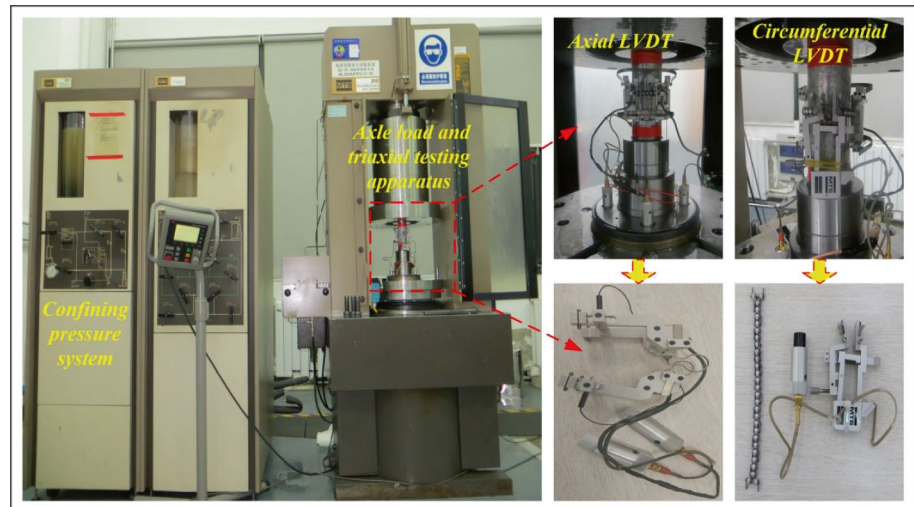
2021). An axial extensometer and chain-type lateral (circumferential) extensometer were provided to collect axial and circumferential deformation data of the rock specimens. Prior to testing, both the upper and lower end surfaces of the specimens were evenly covered with Vaseline (lubricant), to reduce the negative influence of end friction between the bearing plate (indenter) of the testing machine and the rock specimen.

## 2.2 Design of the Testing Program

The strength and deformation characteristics of rock are not only the basis of theoretical calculation and design work, but also one of the important contents of rock mechanics and engineering research. The uniaxial and triaxial compression tests of rocks are important means to obtain rock mechanical parameters. Generally, the compression test of rock can be divided into monotonic loading test and cyclic loading test. The monotonic loading test of rock is to apply axial pressure ( $\sigma_1$ ) or confining pressure ( $\sigma_3$ ) at a certain loading rate until the end of the test. This article adopts a stepwise cyclic loading and unloading test, which is that all the stress is removed when the stress reaches the design value ( $\sigma'$ ). Then, it is reloaded to a higher stress value than the previous unloading



**Fig. 3** MTS 815 rock mechanics test system



point, and then unloaded. The loading and unloading are carried out repeatedly until the rock sample is damaged and the test is terminated. The main reasons for choosing the triaxial cyclic loading and unloading test in this paper are as follows:

1. Rock is a collection of different minerals, which contains cracks, pores and other defects. It is a non-homogeneous and inelastic natural geological material. In the process of compression under load, the axial and circumferential deformation ( $\varepsilon_1, \varepsilon_3$ ) of the rock sample is composed of the elastic deformation of the bearing structure skeleton (mineral), the slip of the fracture surface and the closure of pores. Elastic deformation ( $\varepsilon_e$ ) can be restored after unloading. The closure of the original micro-pores or micro-cracks in the rock sample and the slippage of the fracture surface are deformations that cannot be restored after unloading, which is collectively referred to as plastic deformation ( $\varepsilon_p$ ). Conventional uniaxial and triaxial compression tests cannot separate the strain ( $\varepsilon_1, \varepsilon_3$ ) of the loaded rock sample, and the cyclic loading and unloading test can distinguish the elastic strain ( $\varepsilon_e$ ) and plastic strain ( $\varepsilon_p$ ) of the loaded rock sample. Therefore, the  $\varepsilon_e$  and  $\varepsilon_p$  are separated through the triaxial cyclic loading and unloading test, which provides basic data for the follow-up study on the damage accumulation and expansion characteristics of high-temperature rock samples.
2. Engineering practice shows that underground projects such as roadways (caverns, tunnels) are affected by the construction technology, which makes the stress state of the roadway surrounding rock constantly change. The stress state has roughly gone through the following stages: the original stress state before excavation (equivalent to the initial loading state)  $\rightarrow$  the surrounding rock stress redistribution state caused by the excavation (equivalent to the unloaded state)  $\rightarrow$  stress state

under subsequent excavation or mining stress (loading state)  $\rightarrow$  surrounding rock deformation Stress state (unloading state), cyclically. The force on the pillars is also constantly changing, affected by the mining technology of coal mines: pillars in the original rock stress state before coal mining (loading)  $\rightarrow$  coal recovery in this section (unloading)  $\rightarrow$  stress state under the influence of mining stress during coal mining in other sections (loading)  $\rightarrow$  pillar deformation releasing stress state (unloading), cyclically. Therefore, in the construction process of underground engineering, the rock is often subjected to repeated loading and unloading. The strength, deformation and damage mechanical properties of the rock are closely related to the stress state and the loading form. The micro-cracks in the lower part continue to expand and develop under stress loading, so that the rock damage continues to accumulate, which can eventually lead to the destruction of the rock. The micro-cracks in the rock continue to expand and develop under stress loading (loading process), so that the rock damage continues to accumulate, which can eventually lead to rock destruction. During the unloading process, the previously closed fissures inside the rock may open again, thereby affecting the mechanical properties of the rock. In addition, the surrounding rock of underground engineering (roadways, caverns, tunnels) is in a three-dimensional stress state. Therefore, the selection of the triaxial cyclic loading and unloading path is closer to the actual stress state of the engineering surrounding rock. Simultaneously, the temperature is an important factor affecting the properties of rocks. The physical and mechanical properties of rocks have undergone significant changes after high temperatures.

In view of this, we use the MTS 815 rock mechanics test system to carry out triaxial cyclic loading and unloading

tests on five high-temperature rock samples. We try to reveal the strength, deformation, and expansion characteristics of high-temperature rock samples under triaxial loading and unloading conditions, to deepen the understanding of the strength degradation process and damage mechanism of high-temperature rocks. The research results can provide a theoretical basis for the surrounding rock stability analysis, repair, and reinforcement design of underground engineering after a fire.

Rock compression tests were divided into monotonic loading and cyclic loading testing. In this study, stepwise cyclic loading and unloading testing were applied. When the stress reached the designed value, it was unloaded and removed. The stress was later re-loaded to a value higher than the previous unloading point and then unloaded again. This procedure was repeated until failure of the rock specimen was observed.

Further modifications were important to ensure the success rate of the triaxial cyclic loading and unloading tests, which can fail as a result of post-peak instability of rock with high brittleness after unloading. Therefore, whilst determining the stress path through exploratory testing, a method combining axial displacement loading with axial stress

unloading was adopted to control the process of triaxial cyclic loading and unloading (Fig. 4). The design program for this testing is detailed in Table 1. During the testing process, the axial displacement ( $u_i$ ) control mode was adopted for constant gradient loading. The displacement loading gradient for one cycle (loading and unloading stage) was designed as 0.1 mm, and the  $u_i$  loading rate was 0.003 mm/s. Once the axial displacement was loaded to the design value  $u_s$ ,  $\sigma_1$  was unloaded through axial stress ( $\sigma_1$ ) control, with an unloading rate of  $\sigma_1$  is 2.0 kN/s. This stage was repeated until the remnant stage ( $\sigma_r$ ) of the rock specimen and the completion of the test.

The specific operational procedures of the triaxial cyclic loading and unloading testing of the rock specimens after high-temperature treatment were as follows:

1. Test preparation: The basic dimensional parameters of the rock specimens including length and diameter were measured. Thin thermal shrinkable films were wrapped around the rock specimens to prevent the hydraulic oil from immersing into the failure-state rock specimen. The longitudinal wave velocity of the rock specimens was measured, and high-temperature rock specimens with similar wave velocities were selected for compressive experiments, to reduce the dispersion of the experimental data.
2. At the beginning of testing, the rock specimens were placed at a central position at the base of the triaxial pressure chamber, and a 1.0 kN axial load ( $\sigma_1$ ) was applied for fixation of the rock specimen. This prevented movement of the rock specimen during the application of confining pressure, thus avoiding the impact of eccentric axial pressure on the test data. A  $\sigma_3$  load was applied to the predetermined value (1, 5, 10, 15, 20 MPa) at a loading rate of 0.05 MPa/s. During testing,  $\sigma_3$  remained constant.
3. Stress path for loading and unloading testing:  $d_0$  (initial displacement of the loaded rock specimen was generally 0)  $\rightarrow d_0 + 0.1$  mm (design value  $u_s$  of the axial displacement, loading)  $\rightarrow 0$  (axial stress, unloading)  $\rightarrow d_0 + 0.2$  mm (loading)  $\rightarrow 0$  (unloading)  $\rightarrow d_0 + 0.3$  mm (loading)  $\rightarrow 0$  (unloading)  $\rightarrow \dots \rightarrow$  remnant stage (end of the testing). When the axial load was decreased to 1.0 kN, the unloading ceased

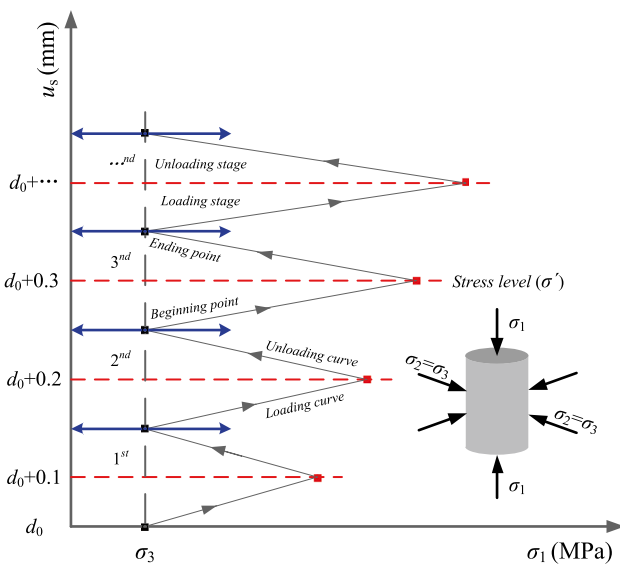


Fig. 4 Stress path for high-temperature treated rock specimens under triaxial cyclic loading—unloading testing

Table 1 Cyclic loading and unloading triaxial compression test of rock specimens

$\sigma_3$ (MPa)	20 °C	200 °C	400 °C	600 °C	800 °C
1	#1, #2, #3	#16, #17, #18	#31, #32, #33	#46, #47, #48	#61, #62, #63
5	#4, #5, #6	#19, #20, #21	#34, #35, #36	#49, #50, #51	#64, #65, #66
10	#7, #8, #9	#22, #23, #24	#37, #38, #39	#52, #53, #54	#67, #68, #69
15	#10, #11, #12	#25, #26, #27	#40, #41, #42	#55, #56, #57	#70, #71, #72
20	#13, #14, #15	#28, #29, #30	#43, #44, #45	#58, #59, #60	#73, #74, #75

and further stages of cyclic testing can be performed to prevent the influence of the indenter of the testing machine on the rock specimen (Meng et al. 2021).

It should be noted that in triaxial cyclic loading and unloading tests, one complete loading and unloading process is called one cycle. The number of a complete loading–unloading process is called cycle index ( $N$ ).

### 3 Analysis of the Testing data

#### 3.1 Characteristics of Stress–Strain Curves and Failure Forms

Figures 5, 6, 7, 8 and 9 shows the stress–strain curves of high-temperature-treated rock specimens and the curves outer envelope following triaxial cyclic loading and unloading tests under different confining pressures. During triaxial cyclic loading and unloading testing, the hysteresis effect appeared in the stress–strain curve of the treated

**Fig. 5** Stress–strain curve under triaxial cyclic loading–unloading testing when  $T=20\text{ }^{\circ}\text{C}$

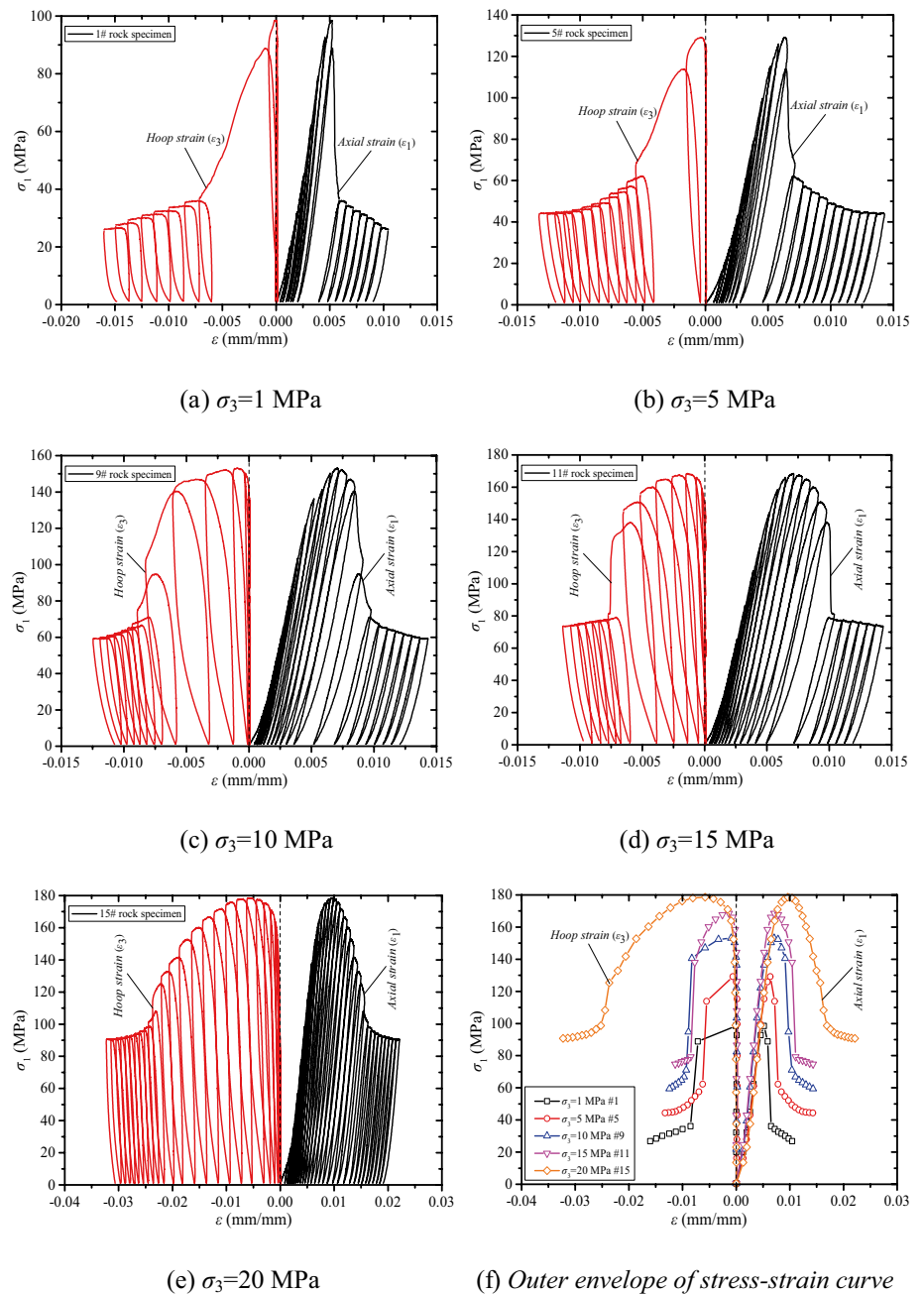
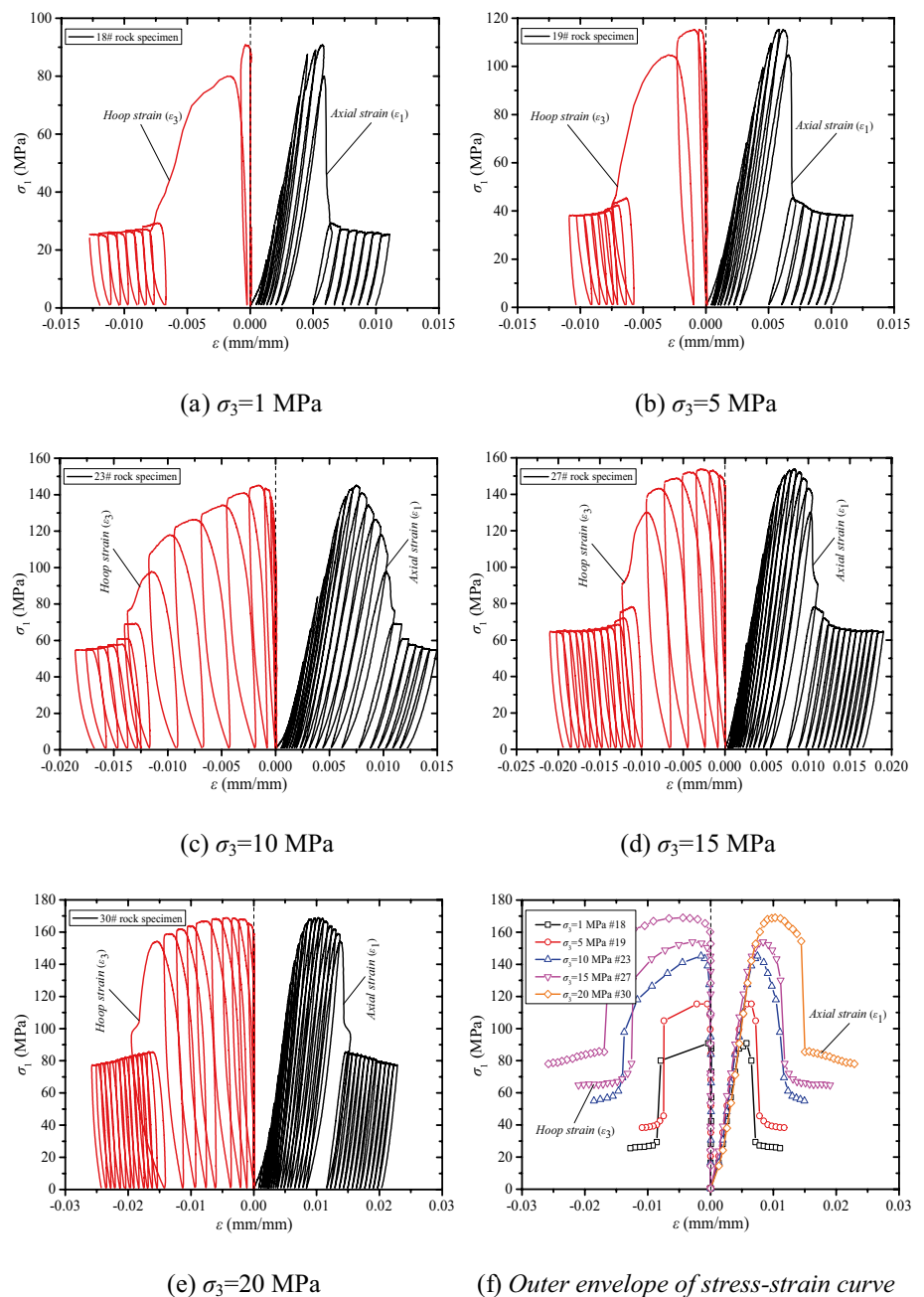


**Fig. 6** Stress–strain curve under triaxial cyclic loading—unloading testing when  $T=200\text{ }^{\circ}\text{C}$

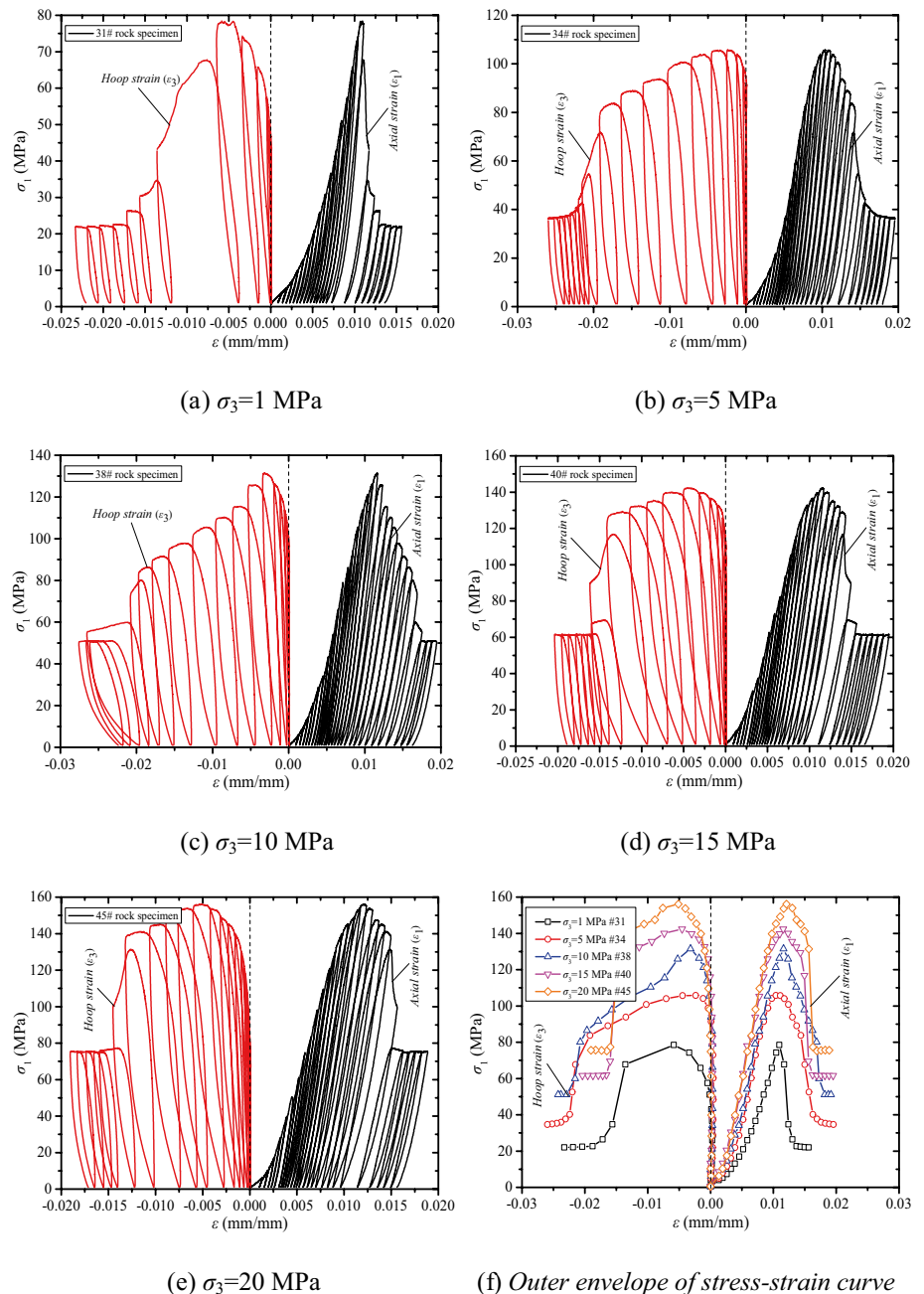


rock specimen, forming a stress–strain closed loop curve. The reason for this was that the rock is a natural geological material containing defects such as micro-cracks, pores and joints. The micro-cracks or pores can close, expand or are interconnected, causing non-ideal elasticity during rock deformation. On one hand, the deformation has the elastic aftereffect, i.e., it requires time for the elastic deformation to recover (hysteretic elastic deformation) while the stress is unloaded. On the other hand, sliding deformation (caused by slipping or flipping displacement of the internal fissure surface or fracture surface) of the rock specimen cannot rapidly recover after unloading. The specimen also enters into

the yielding stage, in which considerable plastic deformation occurs inside the specimen that is not recoverable. The stress was loaded to a certain level ( $\sigma'$ ), and then unloaded. At this moment, the unloading curve did not coincide with the final adjacent loading curve, and was lower, forming a closed circular area (Meng et al. 2016, 2021; Jiang et al. 2018). As the  $\sigma_3$  and  $T$  increase, the number of hysteresis loops also gradually increased.

During loading, the internal brittle region of the rock specimen was initially damaged. With ongoing adjustments, the stress shifted onto the relatively harder bearing framework of the specimen, strengthening its bearing

**Fig. 7** Stress–strain curve under triaxial cyclic loading—unloading testing when  $T=400\text{ }^{\circ}\text{C}$

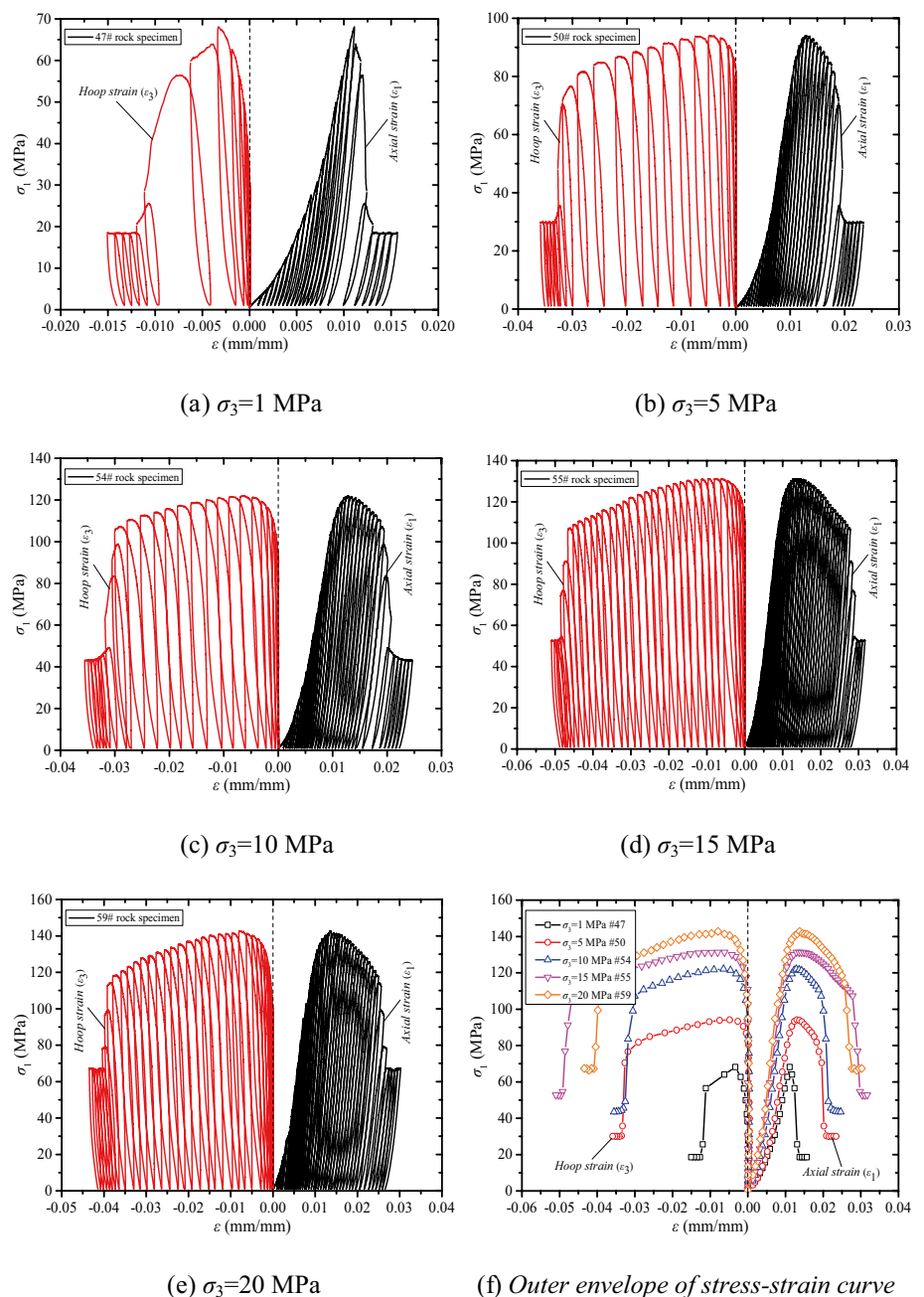


structure. The slope of the reloading curve was therefore larger than that of the last adjacent loading curve. If the reloaded stress did not exceed the level at the last adjacent time of unloading, then the reloading strengthened the bearing structure of the specimen. If the reloaded stress was exceeded, the internal brittle region of the specimen that had not been damaged at the last stress level will undergo damage at the new stress level, making the slope of the stress–strain curve more gentle, and rising along the path of the last adjacent loading curve. This is termed the memory effect of the rock (Meng et al. 2018; Li et al. 2020b).

The failure form of the rock specimen under the load is a key feature for expressing its failure mechanism, which reflects the influence of the testing conditions on the failure mechanisms of the rock (Wong et al. 1997; Wong and Baud 2012; Masri et al. 2014; Yang et al. 2017). There are two major failure forms of the rock specimens under triaxial cyclic loading and unloading. (1) Under low confining pressure, the failure form of the treated rock specimen is an axial splitting failure. In this form, the rock specimen has several vertical splits on its axial surface after failure, which are axially or nearly parallel with the axial direction of the rock specimen. (2) Under the effects of high confining pressure,



**Fig. 8** Stress–strain curve under triaxial cyclic loading—unloading testing when  $T=600\text{ }^{\circ}\text{C}$

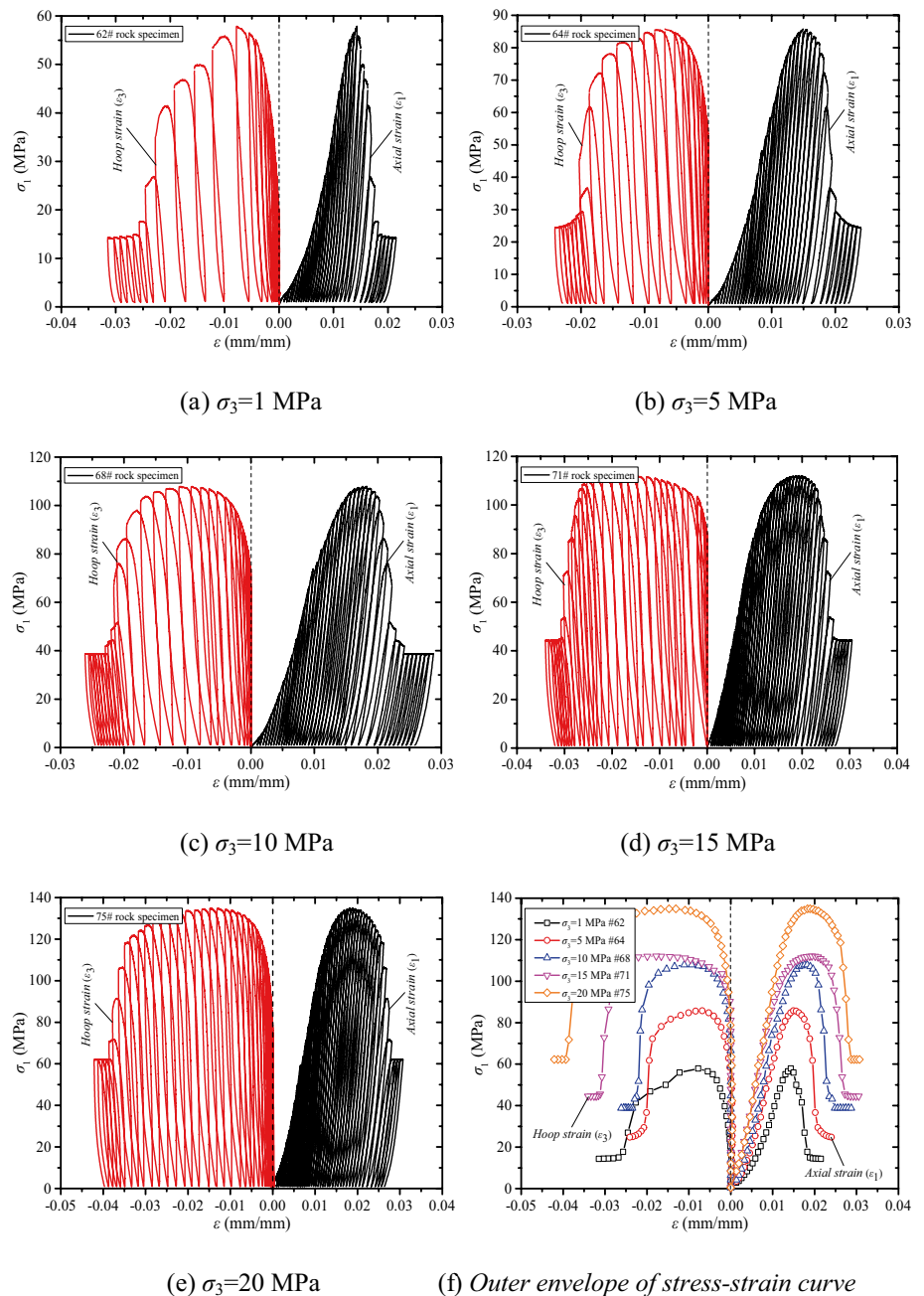


the failure form of the treated rock specimen is a single shear failure. Inside the damaged rock specimen, shearing failure occurs on the surface that runs axially through the majority of the fracture surface and divides the rock specimen into two rock blocks, namely upper and lower.

Shear failure is common under the triaxial compression state. The dip angle of the fracture surface typically represents the fracture angle, which is used to judge the location and direction of the major fracture surface of the rock specimen (Yang et al. 2012; Wei et al. 2019; Meng et al. 2021). Taking  $T=20\text{ }^{\circ}\text{C}$  as the example, when  $\sigma_3=1\text{ MPa}$ ,  $\theta \approx 88^{\circ}$ ; when  $\sigma_3=10\text{ MPa}$ ,  $\theta \approx 68^{\circ}$ , a reduction of 22.73%

occurred; when  $\sigma_3=20\text{ MPa}$ ,  $\theta \approx 64^{\circ}$ , a reduction of 27.27% was observed. Taking  $\sigma_3=20\text{ MPa}$  as the example, when  $T=20\text{ }^{\circ}\text{C}$ ,  $\theta \approx 64^{\circ}$ ; when  $T=400\text{ }^{\circ}\text{C}$ ,  $\theta \approx 62^{\circ}$ , a reduction of 3.13% occurred; when  $T=800\text{ }^{\circ}\text{C}$ ,  $\theta \approx 60^{\circ}$ , a reduction of 6.25% occurred. These data indicate that  $\theta$  decreases with increasing  $\sigma_3$  and  $T$ . As  $\sigma_3$  rises, the circumferential restraining force can effectively inhibit the slippage or flipping of the internal fissure surface or fracture surface of the rock specimen, reducing the severity of rock failure and lowering  $\theta$ . As  $T$  rises, the ductility of the rock specimens is enhanced, which reduces the severity of rock failure and lowers  $\theta$ . Based on the degree of reduction

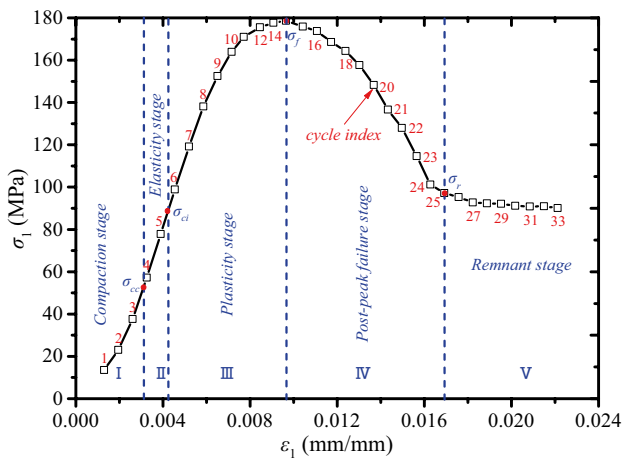
**Fig. 9** Stress–strain curve under triaxial cyclic loading—unloading testing when  $T=800\text{ }^{\circ}\text{C}$



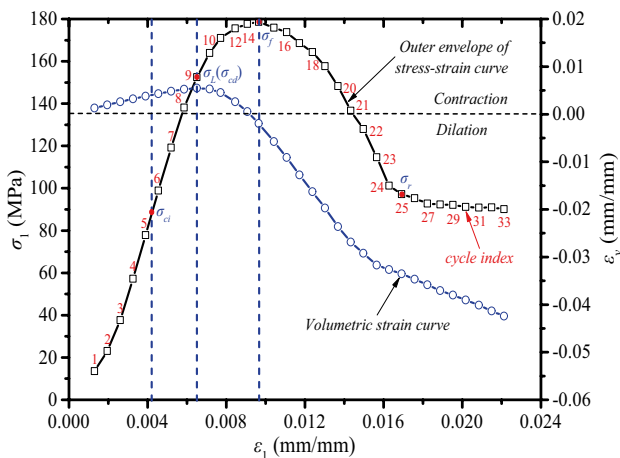
of  $\theta$ , the degree of influence of the confining pressure on the fracture angle is greater than that of the influence of temperature. To summarize, rock failure is controlled by both internal and external factors. Internal factors arise from the non-homogeneity of the rock material and refer to the mineral particles, structure, and formation that constitute the rock. External factors arise from internal non-homogeneous stress as a result of the loading and testing conditions (temperature and water). These lead to the formation of macro-fractures on the surface and change or affect the failure form of the rock specimen.

### 3.2 Characteristics of Outer Envelope of the Stress–Strain Curve

The shape of the outer envelope of the stress–strain curve during triaxial cyclic loading and unloading testing is similar to that of the conventional triaxial compression testing curves. These can be divided into five stages, including compaction, elasticity, plasticity, post-peak failure, and remnants (Bieniawski 1967; Martin and Chandler 1994; Gong et al. 2020; Meng et al. 2020b), as shown in Fig. 10. Compared to the conventional triaxial compression testing



(a) Stages division diagram of outer envelope of stress-strain curve



(b) Critical volume conversion stress ( $\sigma_L$ ) or damage-dilatancy stress ( $\sigma_{ed}$ )

**Fig. 10** Stages of the stress–strain curve and characteristic stress ( $T=20\text{ }^\circ\text{C}$ ,  $\sigma_3=20\text{ MPa}$ )

curve, the outer envelope of the stress–strain curve under the combined action of confining pressure and temperature showed the following differences:

1. **Compaction stage:** micro-cracks or pores inside the rock specimen were gradually compressed under axial and confining pressure, increasing the rigidity of the specimen. This phenomenon was more noticeable in low-strength rocks (soft rock) or rocks with numerous micro-cracks or pores. This was less noticeable for dense rock during this stage. At increasing temperature, the compaction stage is extended, indicating that a higher number of micro-cracks occur inside the specimen as the temperature increases.

2. **Elasticity stage:** as the load increases, the micro-cracks or pores inside the rock specimen are closed, and no new fissures appear. In this case, the stress–strain curve is linear and the deformation of the specimen is elastically recoverable. As the temperature rises, the slope of the stress–strain curve is gentle. When accounting for irreversible deformation (a state of deformation arising from the closure of the compressed micro-cracks or pores inside specimen under a load that not recoverable) of the specimen at the compaction stage, the rock specimen cannot be recovered after unloading, leading to distinct loading and unloading curves.
3. **Plasticity stage:** as the axial load increases, the closed micro-cracks inside the rock specimen reopen and expand. New cracks also appear, resulting in the expansion and interconnection of the internal regions of the specimen. In this case, the growth of the stress–strain curve was non-linear, and the rock specimen shows an apparent non-recoverable plastic deformation. At higher temperatures, the plasticity stage of the rock specimen is extended.
4. **Post-peak failure stage (strain-softening stage):** when the axial load increases to the compressive ultimate strength of the rock specimen, a macro-rupture surface occurs through the interconnection of internal fissures, leading to failure of the rock specimen. In this case, a sharp increase in the deformation of the specimen is observed, coupled to an ongoing decrease in its bearing capacity, resulting in strain softening. As the temperature rises, the downward trend of the stress–strain curve at the post-peak stage is slowed down.
5. **Remnant stage (friction bearing stage):** the rock specimen does not completely lose its bearing capacity following the macro-rupture, though it is damaged under confining pressure conditions. Instead, the bearing capacity decreases to a low-stress level (residual strength, or residual capacity after failure of rock specimen). For this failure, the friction between the rupture surfaces sustains the bearing capacity at the post-peak stage. The residual stress of the specimen increases with the rise of confining pressure but decreases with the rise of temperature.

Under low confining pressures, the stress–strain curve shows a rapid downward trend (noticeable stress drop) when reaches peak stress. The rock specimen loses its bearing capacity in a short period, and brittle failure occurs in the absence of notable signs. As the confining pressure rises, the stress–strain curve approaches peak stress and plastic deformation of the rock specimen increases gradually, during which time the specimen transforms from brittle failure into ductile failure. As the temperature rises, the post-peak stress–strain curve shows a downward trend (gradual stress drop). The brittle

characteristics of the rock specimen become weaker, whilst the plastic characteristics gain strength, reflecting the transformation of brittle failure into ductile failure (Mogi 1972; Wong and Baud 2012; Zhao et al. 2018a; Wei et al. 2019; Meng et al. 2020b). Furthermore, testing of the high-temperature-treated rock is affected by the number of initial defects, including micro-cracks and pores, leading to differences in the test data.

## 4 Discussion

### 4.1 Evolution Rules of Strength Parameters of the Rock Specimen

The strength of a rock refers to the ultimate stress corresponding to a particular state of the rock during the deformation process, including the peak strength (peak stress) and residual strength (residual stress). The strength theory is used to study the failure mechanisms and strength criterion of material under various stress states. As such, the strength or failure criterion represents the relationship between the stress state and strength parameter of the material under the failure conditions. Mohr–Coulomb (M–C) strength criterion is an empirical strength theory built on the statistics and analysis of rock testing data. The M–C strength criterion is not a simple stress state in which the failure of a rock sample occurs, but a combination of different normal stresses ( $\sigma$ ) and shear stress ( $\tau$ ) that the rock loses during its bearing capacity. Specifically, failure occurs when  $\sigma$  and  $\tau$  acting on a certain surface of the rock reach specific values (Lee et al. 2012; Labuz and Zang 2012; Jiang et al. 2018; Renani and Martin 2020). The general expression formula of the M–C strength criterion is given below:

$$\tau = c + \sigma \tan \varphi, \quad (1)$$

where  $\tau$ —shear stress, MPa;  $\sigma$ —normal stress, MPa;  $c$ —cohesion of the rock, MPa;  $\varphi$ —internal friction angle of the rock, °.

The principal stress ( $\sigma_1, \sigma_3$ ) expression adopted in the M–C strength criterion is:

$$\sigma_1 = k\sigma_3 + b = \sigma_3 \frac{1 + \sin \varphi}{1 - \sin \varphi} + \frac{2c \cdot \cos \varphi}{1 - \sin \varphi} = \sigma_3 \cdot \tan^2 \left( \frac{\pi}{4} + \frac{\varphi}{2} \right) + 2c \cdot \tan \left( \frac{\pi}{4} + \frac{\varphi}{2} \right). \quad (2)$$

The strength parameters (cohesion  $c$ , internal fracture angle  $\varphi$ ) of the rock and theoretical value of the rupture angle to be obtained are:

$$\begin{cases} c = b/2\sqrt{k} \\ \varphi = \arcsin[(k-1)/k+1], \\ \theta = \frac{\pi}{4} + \frac{\varphi}{2} = 45^\circ + \frac{\varphi}{2} \end{cases} \quad (3)$$

where  $k, b$ —strength parameters;  $\theta$ —fracture angle of the rock, °.

The curve showing the relationship between strength parameters of the high-temperature-treated rock specimen and the confining pressure and temperature are shown in Fig. 11. When  $T=20$  °C,  $c_f=25.51$  MPa (peak cohesion),  $\varphi_f=37.56^\circ$  (peak internal friction angle);  $c_r=7.35$  MPa (residual cohesion),  $\varphi_r=32.13^\circ$  (residual internal friction angle). When  $T=400$  °C,  $c_f=21.35$  MPa,  $\varphi_f=36.72^\circ$ ;  $c_r=6.17$  MPa,  $\varphi_r=28.02^\circ$ . When  $T=800$  °C,  $c_f=15.97$  MPa,  $\varphi_f=35.27^\circ$ ;  $c_r=4.09$  MPa,  $\varphi_r=24.11^\circ$ . These data indicate that the bearing capacity ( $\sigma_f, \sigma_r$ ) and strength parameters ( $c, \varphi$ ) of the rock specimen increase with the rise of  $\sigma_3$ , leading to an enhancement effect of confining pressure. The bearing capacity and strength parameters decrease with the rise of  $T$ , indicative of a temperature deterioration effect.

As  $\sigma_3$  rises, the simultaneous constraining force provided by the confining pressure ( $\sigma_3$ ) and axial stress ( $\sigma_1$ ) suppress slippage of the fissure or fracture surface of the rock specimen, further improving the bearing ( $\sigma_f, \sigma_r$ ) and anti-deformation capacity (elastic modulus  $E$ ). On one hand, fissures inside the rock specimen show a higher degree of interconnection as a result of mineral dehydration, lattice reorganization, mineral shrinkage, and decomposition under high temperatures. Due to the continuous expansion and interconnection of original fissures and the emergence of new cracks, the compaction and integrity of the specimen decrease, influencing both the physical and mechanical properties (Heuze 1983; Ranjith et al. 2012; Sun et al. 2016; Yang et al. 2017; Meng et al. 2020a). On the other hand, thermal stress concentration emerges locally between the mineral particles on account of their different thermal expansion coefficient and anisotropy of thermal expansion inside the minerals under the influence of temperature. This concentration leads to changes to the internal structure of the particles, causing new fissures on the boundary or inside the particles, enhancing the formation of a fissure, thereby affecting the deformation and bearing performance of the rock specimen. From a macroscopic perspective, the dete-

rioration of the mechanical properties of the rock specimen is expressed through the reduction of its bearing ( $\sigma_f, \sigma_r$ ) and anti-deformation capacity ( $E$ ).

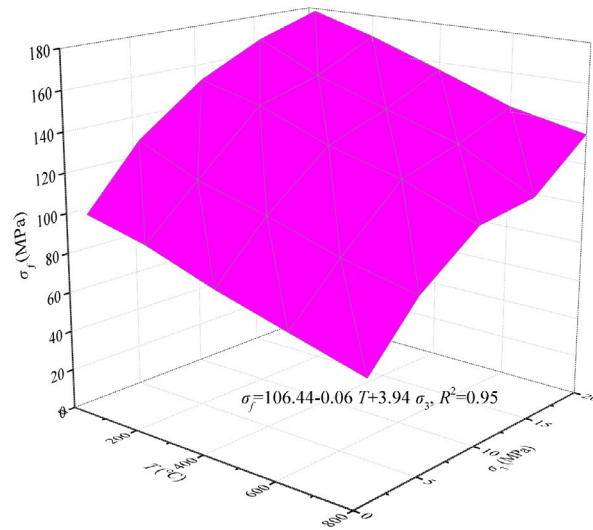
### 4.2 Evolution Rules of Deformation Parameters of the Rock Specimen

#### 1. Stress parameters

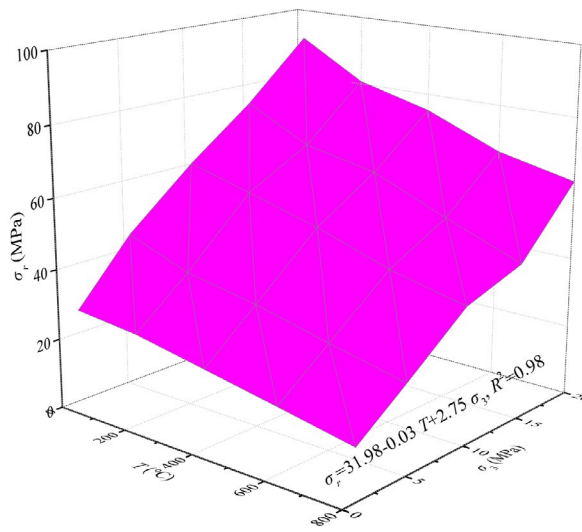
Deformation refers to a change in the volume and shape of rocks in response to stress. Rocks display



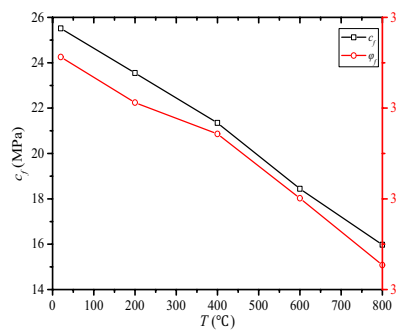
**Fig. 11** The relationship between the strength parameters of the high-temperature-treated rock specimen and the confining pressure/temperature



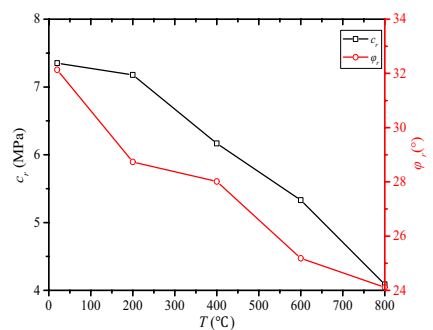
(a)  $\sigma_f - T$  and  $\sigma_3$



(b)  $\sigma_r - T$  and  $\sigma_3$



(c)  $c_f, \phi_f - T$



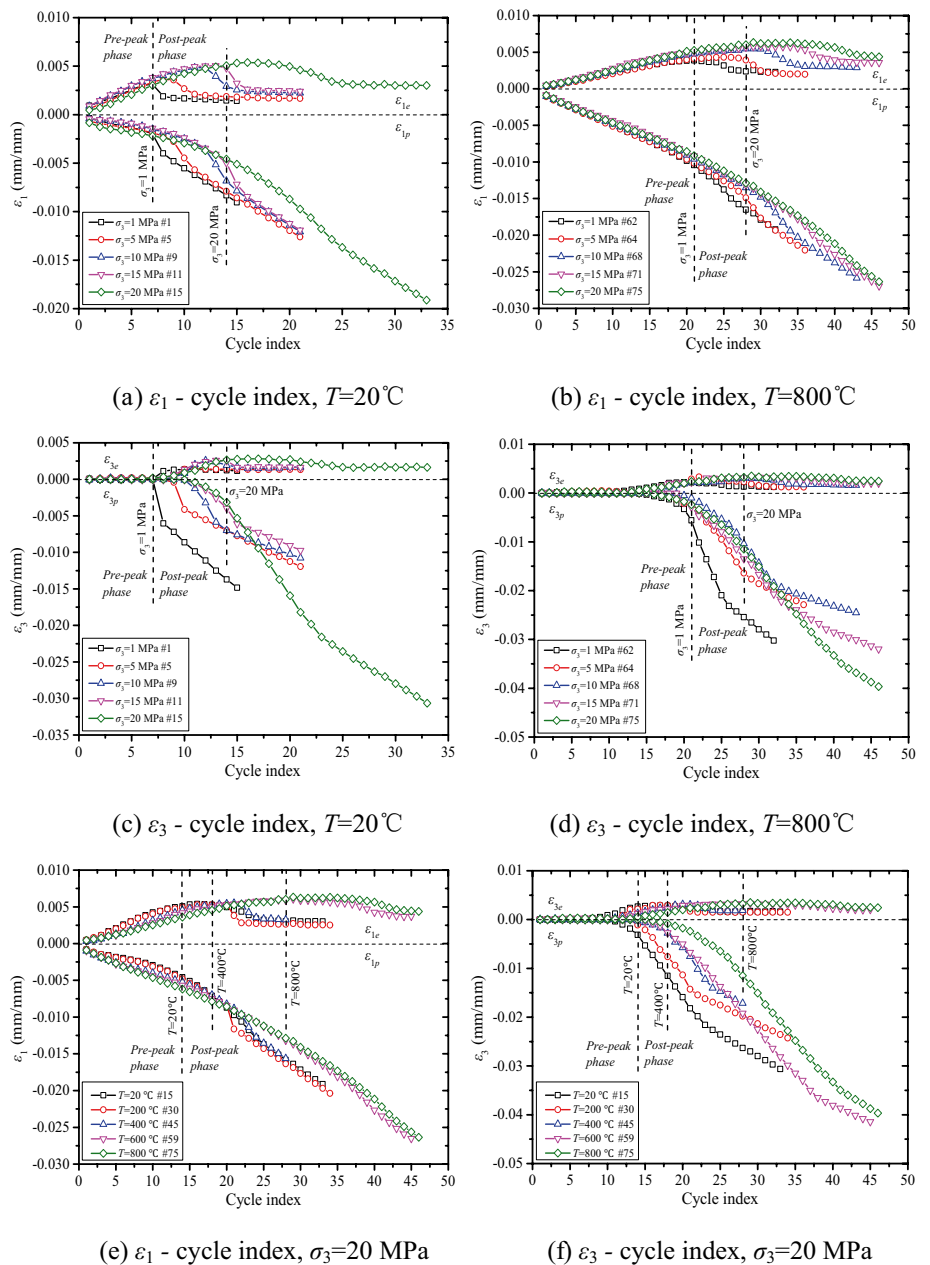
(d)  $c_r, \phi_r - T$

elastic and plastic deformation characteristics. During triaxial cyclic loading and unloading processes, the total strain ( $\epsilon_1, \epsilon_3$ ) of a loaded rock specimen includes the elastic ( $\epsilon_{1e}, \epsilon_{3e}$ ) and plastic strain ( $\epsilon_{1p}, \epsilon_{3p}$ ). Elastic deformation is recoverable after unloading, whilst plastic deformation cannot be recovered. The plastic deformation of loaded rock specimens can be classed as deformation arising from the closure of compressed micro-cracks or pores inside the specimen, or deformation arising from slippage or flipping of the internal fissure or fracture surface. The evolution rules of axial and circumferential strains of high-temperature-treated rock

specimens under triaxial cyclic loading and unloading tests are shown in Fig. 12.

Figure 12 shows that the axial and circumferential strains ( $\epsilon_1, \epsilon_3$ ) of the loaded rock specimen increased with the cycle index. As  $\sigma_3$  and  $T$  rise, the  $\epsilon_p$  of the rock specimen increased accordingly. These results indicate that the deformation of rock following exposure to high-temperature treatment has the characteristics of elastic aftereffects (elastic hysteresis effect). In other words, most elastic deformation that has occurred during stress unloading can be immediately recovered (instantaneous elastic deformation), whilst elastic deformation requires time for recovery (hysteretic elastic deformation). The

**Fig. 12** Evolution rules of axial and circumferential strains of high-temperature-treated rock specimens under triaxial cyclic loading—unloading testing



instantaneous elastic deformation of rock specimens is caused by the compression of internal solid particles and can be reflected by changes in volume. The elastic aftereffect is related to the friction between the internal closed micro-cracks. As the deformation direction of the rock specimen at the time of loading differs to the time of unloading, the force of friction between micro-cracks must be overcome for deformation. Time is required to overcome the friction, meaning the unloading curve is steep during the early stages and more gentle at later stages. Plastic deformation of the rock specimen is caused by the relative slippage between mineral lattices or clay mineral aggregates, with such slippages being irreversible. Plastic deformation is therefore not recoverable. Due to the existence of hysteretic elastic and plastic deformation, the unloading curve at any point on the stress–strain curve of the rock specimen does not coincide with the loading curve in the same cycle. It also does not correlate with the re-loading curve in the final adjacent cycle. Therefore, a closed loop (hysteresis loop) is formed between the unloading curve and re-loading curve, as shown in Figs. 5, 6, 7, 8 and 9.

A rock is an aggregate of one or more minerals that is not homogeneous or elastic. It contains some initial defects, such as micro-cracks or pores, making its internal strength unequal upon loading. Generally speaking, the internal regions of a low-strength rock are first to yield under a stress load. As  $\sigma_3$  rises, the axial stress ( $\sigma_1$ ) increases the occurrence of plastic deformation, forcing the internal regions of higher strength to also gradually yield. More than one yield plane subsequently appears inside the rock specimen, expressed as a continuous increase in plastic deformation, with the stress–strain curve transforming from brittle into ductile failure (Wei et al. 2019; Yang et al. 2012; Meng et al. 2017, 2020a; Zhang et al. 2020). Following high-temperature treatment, the rock specimen experiences the effects of hot melting, tearing and thermal decomposition, for which the occurrence of internal micro-cracks increases, the rigidity of cement decreases, and the deformation of the rock specimen becomes more intensified. Differences in the particle composition and arrangement of the minerals inside the rock specimen, therefore, lead to non-uniform deformation of the internal particles after high-temperature treatment. The mutual squeezing of particles influences the deformation rules of the rock specimen, leading to a gradual increase in plastic deformation. The downward trend of the post-peak stress–strain curve is gentle and the rock specimen shows marked ductile deformation, indicating that the  $\varepsilon_p$  of the rock specimen increases with rising temperature.

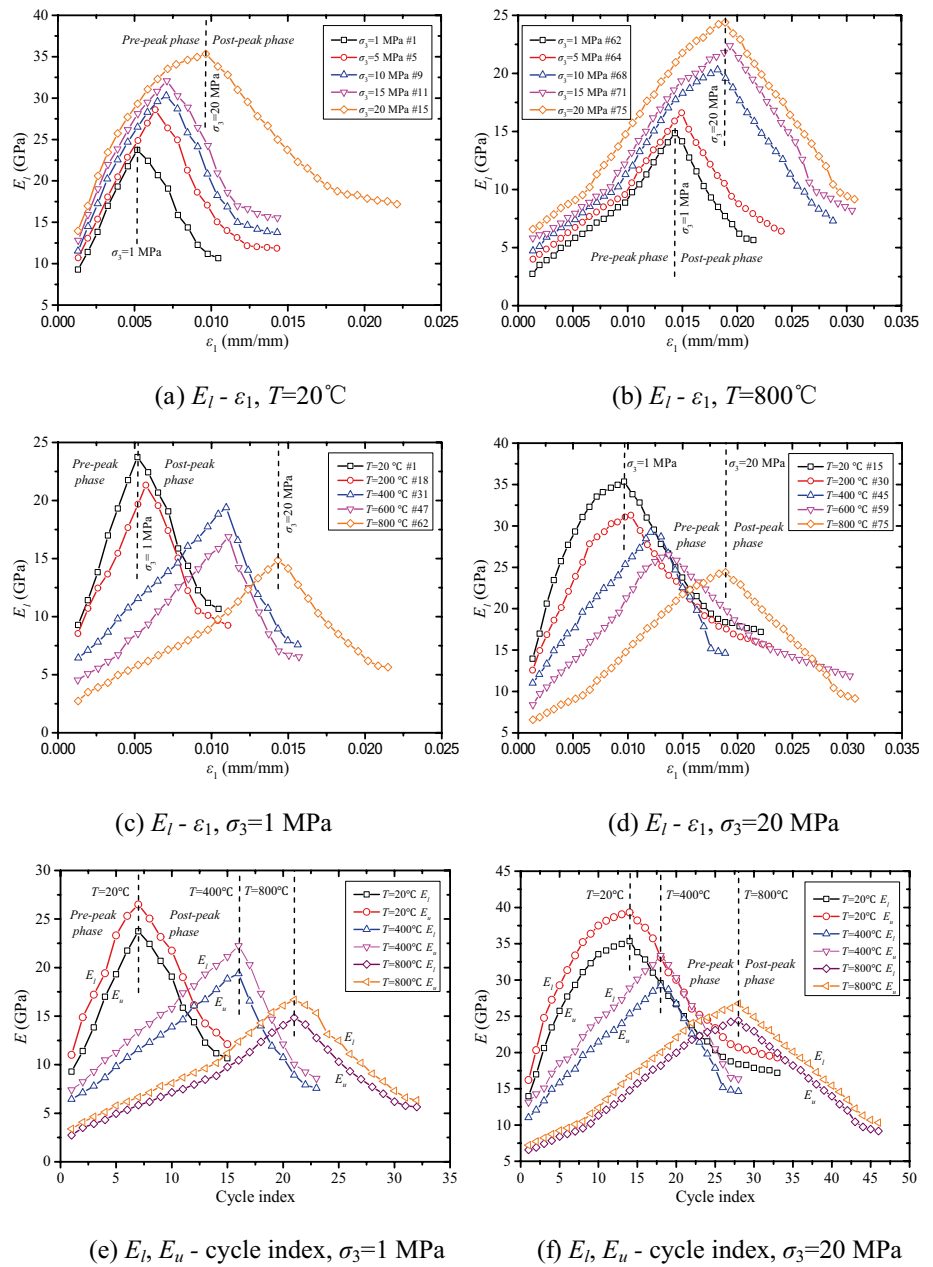
## 2. Evolution rules of elastic modulus

Elastic modulus ( $E$ ) is a major parameter expressing the deformation of a loaded rock specimen that reflects the stress–strain relation under the compressed state. Its value varies with stress–strain curve and deformation stages. As rocks have an elastic aftereffect, a hysteretic loop exists that can be expressed by the loading ( $E_l$ ) and unloading modulus ( $E_u$ ).  $E_l$  can characterize the slope of the elastic section of the loading curve,  $E_u$  can characterize the slope of an elastic section of the unloading curve. Using the elastic modulus calculation under cyclic loading and unloading testing proposed by Meng et al. (2018), the evolution of loading and unloading moduli of high-temperature-treated rock specimens under triaxial cyclic loading and unloading testing can be revealed. Figure 13 shows that when the cycle index or  $\varepsilon_1$  increases,  $E_l$  and  $E_u$  initially increase and then decline. This is identical to the changing trend of bearing capacity of the rock specimen (at the pre-peak stage, when cycle index or  $\varepsilon_1$  increases, the bearing capacity of rock specimen increases; at the post-peak stage, when cycle index or  $\varepsilon_1$  increases, the bearing capacity gradually decreases as a result of residual stress). With the rise of  $\sigma_3$ , both  $E_l$  and  $E_u$  increase and  $E_u$  is higher than  $E_l$ ; with the rise of  $T$ , both  $E_l$  and  $E_u$  decrease.

At the pre-peak stage, the slope ( $E_l$ ) of the unloading curve in each cycle and the slope ( $E_u$ ) of the re-loading curve in the last adjacent cycle are larger than that ( $E_l$ ) of the loading curve in that cycle. This suggests that the capacity of the rock specimen increases with the increasing cycle index, exhibiting strain-hardening characteristics. The reasons for this are as follows: (1) during the pre-peak compaction and elasticity stage, the micro-cracks or pores inside the rock specimen are closed under a load (axial pressure and confining pressure), and new micro-cracks arising from local stress concentration have yet to emerge or be expanded completely, increasing the degree of compaction and bearing capacity of the rock specimen. (2) At the pre-peak plasticity stage, rock debris as a result of shearing and slippage of the fissure or fracture surface may fall off during unloading and enter into the adjacent pores or fissures. Their entry increases the force of friction between fissures or fractures, and allows the irregular fissure or fracture surface to effectively disperse the stress. As a result, the stress inside the rock tends to be uniformly distributed and the bearing capacity increases, showing a growing trend of  $E_l$  and  $E_u$  with the rise of cycle index.

At the post-peak stage, the slopes ( $E_l$ ,  $E_u$ ) of loading and unloading curves decrease with the rise of the cycle index, indicating that the resistance of the rock specimen to deformation decreases with increasing damage, revealing strain-softening characteristics. This can be explained as during the post-peak failure and remnant stages,

**Fig. 13** The relationship between the loading—unloading moduli of the high-temperature-treated rock specimens and confining pressure/temperature



micro-cracks, run-through fissures or macro-fracture surfaces inside the rock specimen occur. During subsequent reloading, these internal micro-cracks continue to expand, become interconnected, or the run-through of the fissures or the macro-fracture surfaces slip or flip, increasing the damage or failure stage of the rock specimen. As the deformation is sharply intensified and the bearing capacity is decreased,  $E_l$  and  $E_u$  decrease with the rise of the cycle index.

To summarize, as  $\sigma_3$  rises, the peak stress, residual strength, and resistance to deformation of the rock specimen increase, resulting in higher  $E_l$  and  $E_u$  with the rise of  $\sigma_3$ . As  $T$  rises, the bearing capacity and resistance to deformation

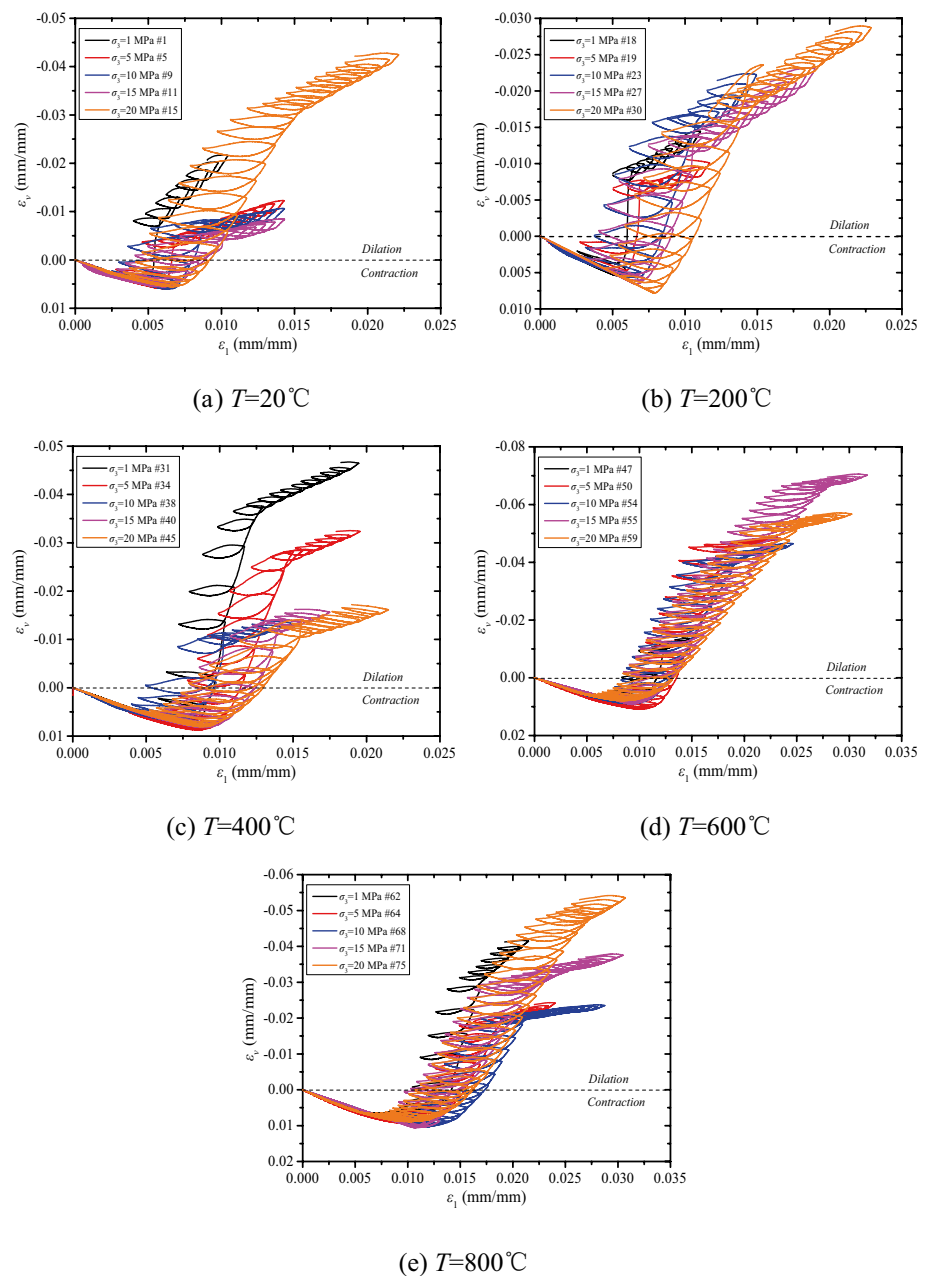
of the rock specimen decreases, leading to a decrease of  $E_l$  and  $E_u$  with the rise of  $T$ .

### 4.3 Evolution Rules of Dilatancy Characteristics

The deformation characteristics of the rock specimen are reflected by the evolution rules of volume strain ( $\epsilon_v$ ). In this study, Figs. 14 and 15 show the evolution rules of the volume strain of high-temperature treated rock specimens under triaxial cyclic loading and unloading testing. (1) The critical volume conversion stress ( $\sigma_1$ ) at which the volume strain changes from compression deformation to dilatancy is taken as the demarcation point. When the load applied ( $\sigma_1$ )



**Fig. 14** The volume strain-axial strain relation of high-temperature-treated rock specimen under triaxial cyclic loading—unloading testing

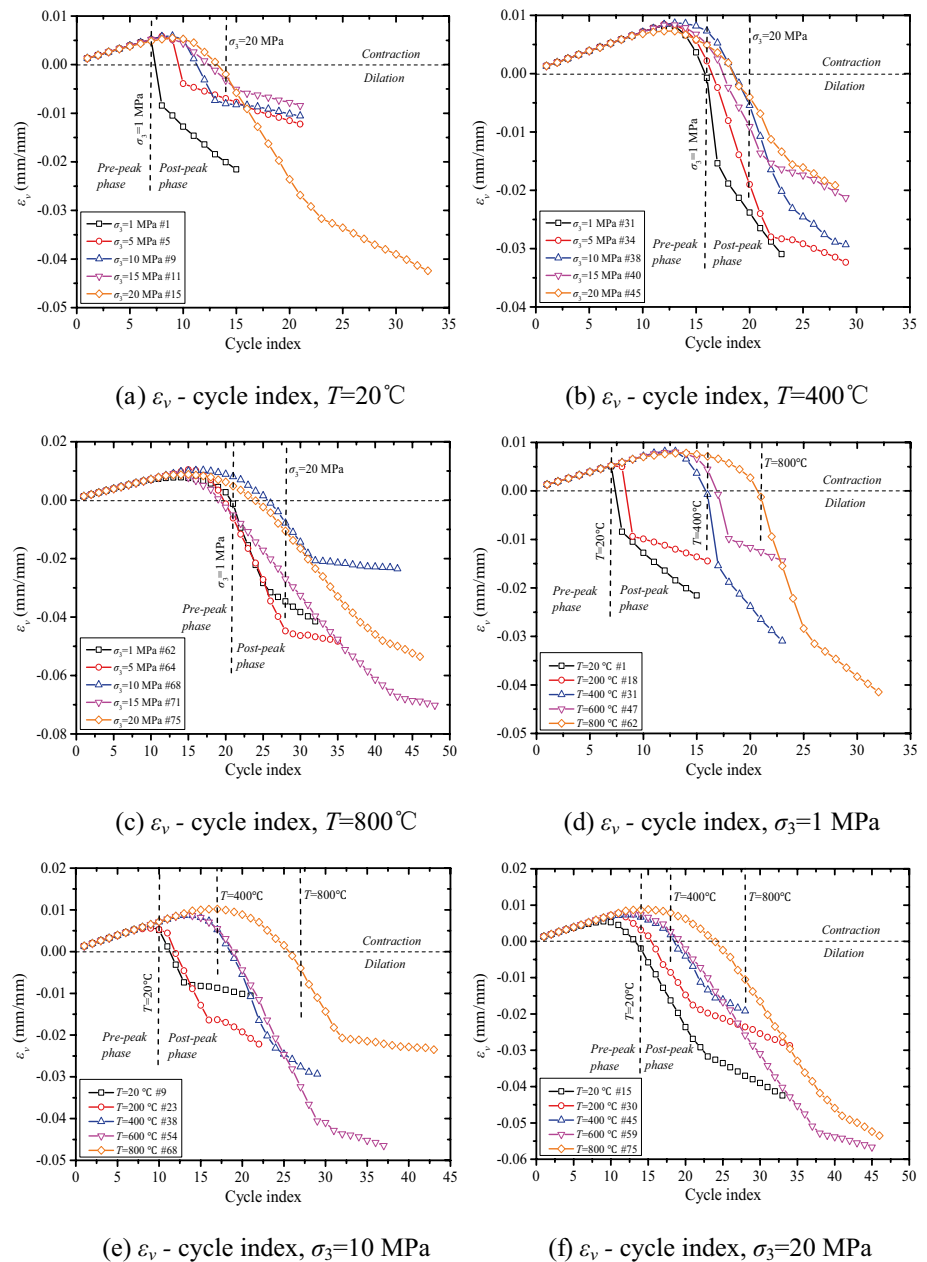


is less than  $\sigma_L$ , the volume strain of the rock specimen is in the state of compression deformation. The volume of the rock increases and then declines with the rise of the cycle index. When the load applied ( $\sigma_1$ ) exceeds  $\sigma_L$ , the volume strain of rock specimen changes from compression deformation to dilatancy, and the rock specimen undergoes irreversible volume expansion. (2) Taking  $T=20^{\circ}\text{C}$  as the example, when  $\sigma_3=1\text{ MPa}$ ,  $\sigma_L=98.49\text{ MPa}$ ; when  $\sigma_3=10\text{ MPa}$ ,  $\sigma_L=153.15\text{ MPa}$ ; when  $\sigma_3=20$ ,  $\sigma_L=178.62\text{ MPa}$ . When  $\sigma_3=1\text{ MPa}$  rises to  $20\text{ MPa}$ , the loading and unloading cycle index in which the dilatancy occurs increases from the 8th to the 14th. Taking  $\sigma_3=20\text{ MPa}$  as the example, when  $T=20^{\circ}\text{C}$ ,  $\sigma_L=178.62\text{ MPa}$ ; when  $T=400^{\circ}\text{C}$ ,

$\sigma_L=151.76\text{ MPa}$ , with a reduction of 15.04%; when  $T=800^{\circ}\text{C}$ ,  $\sigma_L=132.86\text{ MPa}$ , with a reduction of 25.62%. When  $T=20^{\circ}\text{C}$  rises to  $800^{\circ}\text{C}$ , the loading and unloading cycle index in which the dilatancy occurs increases from the 14th to the 24th.

During the loading process, the internal micro-cracks open, expand and become interconnected with each other to form a macro-fracture surface. With the growth of internal fissures, the volume strain of the rock specimen increases and manifests as volume expansion from the macroscopic view. With the rise of  $\sigma_3$ , the bearing capacity of rock specimen keeps increasing, and the post-peak volume strain curve becomes less steep (the changing rate

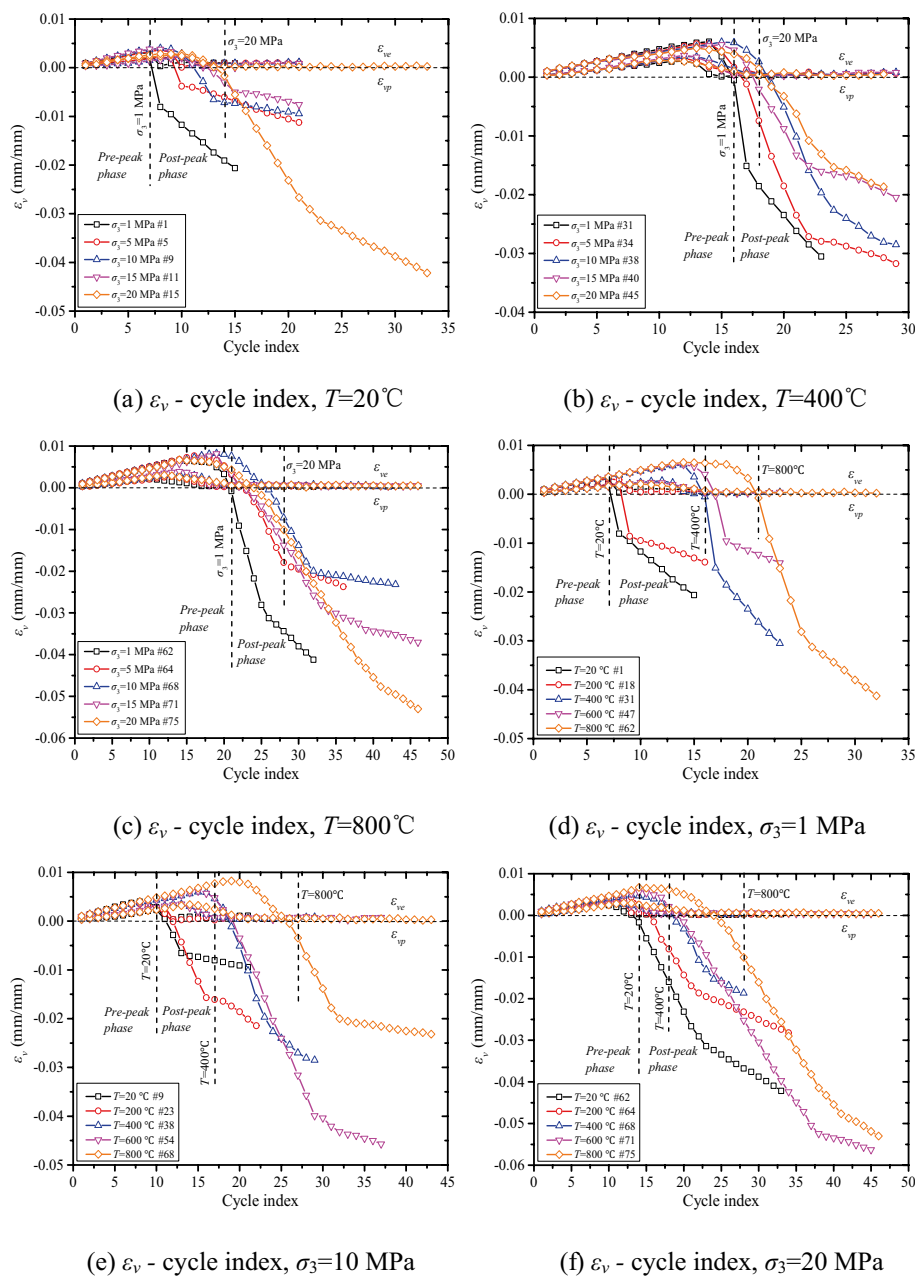
**Fig. 15** The volume strain evolution of high-temperature-treated rock specimen under triaxial cyclic loading—unloading testing



of volume strain decreases). The emergence of dilatancy is delayed by the increase in  $\sigma_L$  necessary for the conversion of the rock specimen from compression deformation to latency, and the increase in the compression deformation prior to dilatancy. This indicates that the confining pressure has an inhibitory effect on the dilatancy deformation of the rock specimen. With the rise of  $T$ , the strength of rock specimens deteriorates, leading to decreased  $\sigma_L$ . When the plastic deformation of the rock specimen is enhanced, the post-peak volume strain curve becomes gentle, and the compression deformation prior to dilatancy increases, which generally delays the emergence of dilatancy.

The relationship between volume strain of high-temperature treated rock specimens and confining pressure and temperature under triaxial cyclic loading and unloading testing are shown in Fig. 16. The volume strain of the rock can be divided into elastic ( $\varepsilon_{ve}$ ) and plastic volume strain ( $\varepsilon_{vp}$ ),  $\varepsilon_{ve}$  is composed of recoverable elastic strain ( $\varepsilon_{1e}$ ,  $\varepsilon_{3e}$ ),  $\varepsilon_{vp}$  is composed of irreversible plastic strains ( $\varepsilon_{1p}$ ,  $\varepsilon_{3p}$ ). Taking  $T=20^\circ\text{C}$  as the example, from the pre-peak stage to the post-peak stage,  $\varepsilon_{ve}$  decreases by 1.99–4.23 fold, while  $\varepsilon_{vp}$  increases by 11.7–45.0 fold. The dilatancy volume strain of the rock specimen is larger than the compression volume strain (1.34–3.66 fold-change). With the

**Fig. 16** The relationship between volume strains of the high-temperature-treated rock specimen and confining pressure/temperature under triaxial cyclic loading—unloading testing



rise of cycle index and  $T$ , irreversible plastic deformation increases. The elastic volume strain ( $\epsilon_{ve}$ ) of the rock specimen therefore initially increases, and then declines, reaching its maximum value prior to dilatancy. The value of  $\epsilon_{ve}$  at the residual stage is minimal. With the rise of the cycle index and  $T$ , the plastic volume strain of the rock specimen gradually increases, making the post-peak volume strain curve gentle, delaying the emergence of dilatancy. Since the confining pressure can effectively inhibit the slippage of the internal fissure surface or fracture surface, the plastic volume strain ( $\epsilon_{vp}$ ) of rock specimen shows a downward trend with the rise of  $\sigma_3$ .

#### 4.4 Evolution Rules of the Brittleness Index of Rock Specimens

Rock failure refers to the phenomenon of instability occurring when a load reaches its ultimate bearing capacity. It can be divided into two distinct macro-deformation modes: brittle failure and ductile failure, according to the size of deformation at the time of rock failure (Mogi 1972; Nygård et al. 2006; Zhao et al. 2018b). Brittle failure means that once a rock bears a load, it undergoes failure and loses its bearing capacity in the face of minor deformation (during which the rock does not show the characteristics of plastic deformation). Ductile failure means that a rock can bear

large plastic deformation with minimal loss of its bearing capacity.

The brittleness index or degree of ductility are used to express the macro-failure form of a loaded rock specimen, and thus different forms of brittleness index for the stress, strain, and energy can be established (Hucka and Das 1974; Hajiabdolmajid and Kaiser 2003; Ai et al. 2016). The brittleness index reflects the rate (degree of post-peak stress drop) of how a rock bearing capacity decreases to the residual strength after failure. The value of the brittleness index ( $B_s$ ) is associated with the slope of the post-peak stress–strain curve and the residual strength. The larger the slope (absolute value) of the post-peak stress–strain curve, the stronger the degree of post-peak failure brittleness. Regarding ideal plastic material,  $\sigma_p = \sigma'_1$ ,  $B_s = 0$ . Regarding rock-like post-peak strain-softening material, smaller the  $B_s$  is suggestive of a stronger ductility; larger  $B_s$  is associated with stronger brittleness.

$$B_s = \frac{\sigma_f - \sigma'_1}{\sigma_f}, \quad (4)$$

where  $\sigma_f$ —peak stress, MPa;  $\sigma'_1$ —maximum post-peak stress in each loading and unloading cycle, MPa.

Under triaxial cyclic loading and unloading testing, the rules of the brittleness index of rock specimens evolving with confining pressure and temperature are shown in Fig. 17. The number of post-peak stress drops ( $N_s$ ) can be described as the post-peak cycle index (number of stress drops) that must be completed when the peak stress falls to the residual stress. The difference between  $\sigma_f$  and  $\sigma'_1$  becomes larger, resulting in increased  $N_s$  and  $B_s$ . Under the same temperature, the slope of  $B_s$ – $N_s$  curves gradually decreases with the rise of confining pressure.  $B_s$  decreases with the increase of  $\sigma_3$ . Under the same confining pressure,  $B_s$  slowly increases with the rise of  $T$ . The brittleness index ( $B_s$ ) when the peak stress ( $\sigma_f$ ) drops to the residual stress ( $\sigma_r$ ) is termed the maximum stress drop coefficient ( $B_{rs}$ ). Taking  $T = 20^\circ\text{C}$  as the example, when  $\sigma_3 = 1$  MPa,  $B_{rs} = 0.69$ ; when  $\sigma_3 = 10$  MPa,  $B_{rs} = 0.59$ , a reduction of 14.49% occurs; when  $\sigma_3 = 20$  MPa,  $B_{rs} = 0.48$ , a reduction of 30.44% occurs. Taking  $\sigma_3 = 20$  MPa as the example, when  $T = 20^\circ\text{C}$ ,  $B_{rs} = 0.48$ ; when  $T = 400^\circ\text{C}$ ,  $B_{rs} = 0.51$ , a reduction of 6.25% occurs; when  $T = 800^\circ\text{C}$ ,  $B_{rs} = 0.54$ , a reduction of 12.50% observed.

These data show that under low confining pressure, the post-peak stress shows a large and rapid decline, manifested by a steep post-peak stress–strain curve, and fewer post-peak cycles.  $B_s$  increases rapidly with the increase of  $N_s$ , and the brittle failure of the rock sample becomes more obvious. With the increase of  $\sigma_3$ , the downward trend of the stress–strain curve in the post-peak stage slows down significantly, indicating that the plastic deformation is enhanced, and the number of cycles following the peak of the rock

sample gradually increases, making  $B_s$  slowly increase with increasing  $N_s$ . This is because confining force provided by the confining pressure ( $\sigma_3$ ) and axial stress ( $\sigma_1$ ) effectively restrain the slippage of the fracture surface inside the rock sample, increasing the residual stress ( $\sigma_r$ ) of the rock sample, which reduces the differential value between peak stress ( $\sigma_f$ ) and residual stress ( $\sigma_r$ ). Namely,  $B_s$  and  $B_{rs}$  decrease with increasing  $\sigma_3$ . As the temperature increases, the physical and mechanical properties of the rock sample become altered. Plastic deformation improves and the number of post-peak cycles significantly increases.  $B_s$  increases slowly with increasing temperature. These data indicate that as the temperature increases, the strength and load-bearing performance of the rock sample gradually decline. This causes the differential values between the peak stress ( $\sigma_f$ ) and residual stress ( $\sigma_r$ ) to increase. Namely,  $B_{rs}$  rapidly increases with increasing  $T$ .

Generally, damage parameters can be used to quantitatively describe the damage accumulation in the whole process of deformation to failure of the loaded rock sample. The expression of damage variable with plastic volumetric strain (Martin and Chandler 1994; Eberhardt et al. 1999; Liu et al. 2016):

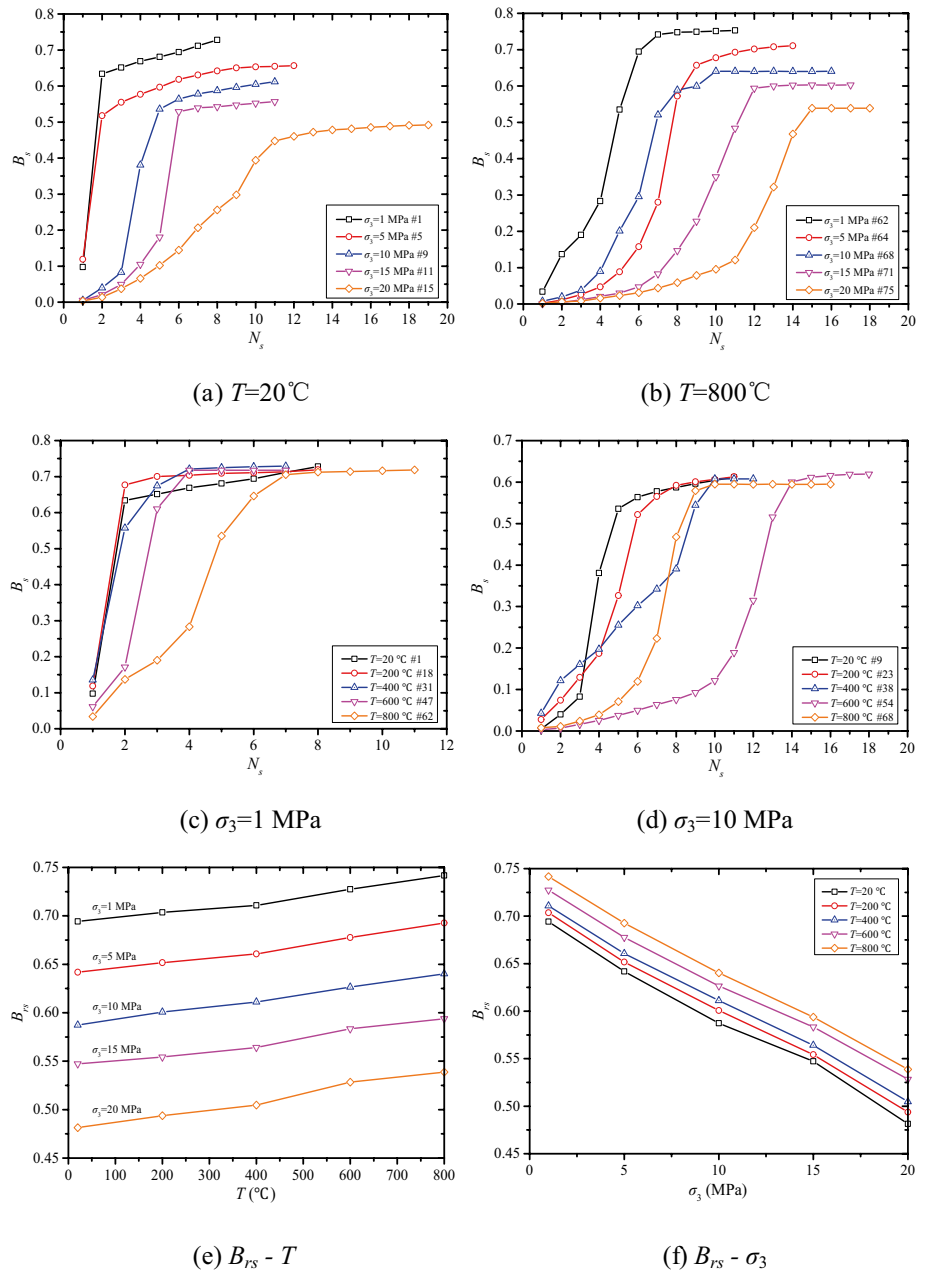
$$D = \varepsilon_{vi}^p / \sum_{i=1}^n \varepsilon_{vi}^p, \quad (5)$$

where  $D$ —the damage variable;  $\varepsilon_{vi}^p$ —the volumetric plastic strain generated by the  $i$ -cycle rock sample, mm/mm;  $\sum_{i=1}^n \varepsilon_{vi}^p$ —the total volume plastic strain generated by rock samples, mm/mm. The damage variable evolution curves of high-temperature rock samples under confining pressure and temperature are shown in Fig. 18.  $D_{pre}$  is defined as the ratio (percentage) of cumulative damage (plastic volumetric strain) to total damage (plastic volumetric strain) of rock samples in the pre-peak stage,  $D_{pos}$  is defined as the ratio (percentage) of cumulative damage to total damage in post-peak rock samples. Taking  $T = 20^\circ\text{C}$  as an example, when  $\sigma_3 = 1$  MPa,  $D_{pre} = 6.48\%$ ,  $D_{pos} = 93.52\%$ ; when  $\sigma_3 = 10$  MPa,  $D_{pre} = 13.93\%$ ,  $D_{pos} = 86.07\%$ ; when  $\sigma_3 = 20$  MPa,  $D_{pre} = 66.42\%$ ,  $D_{pos} = 33.58\%$ . Taking  $\sigma_3 = 20$  MPa as an example, when  $T = 20^\circ\text{C}$ ,  $D_{pre} = 66.42\%$ ,  $D_{pos} = 33.58\%$ ; when  $T = 400^\circ\text{C}$ ,  $D_{pre} = 32.88\%$ ,  $D_{pos} = 67.12\%$ ; when  $T = 800^\circ\text{C}$ ,  $D_{pre} = 15.23\%$ ,  $D_{pos} = 84.77\%$ . It can be seen from Fig. 18 and the above data analysis that:

1. From process from the pre-peak stage to the peak stress point ( $\sigma_p$ ) is the development, connection, penetration of micro-cracks inside the rock sample to the formation of macro-cracks or fracture surfaces, the bearing capacity of the rock sample increases first and then decreases, and the rock sample is not destroyed (the rock sample is still a relatively complete whole) and loses its bearing



**Fig. 17** Rules of brittleness index of the high-temperature-treated rock specimen evolving with the confining pressure and temperature under triaxial cyclic loading—unloading testing

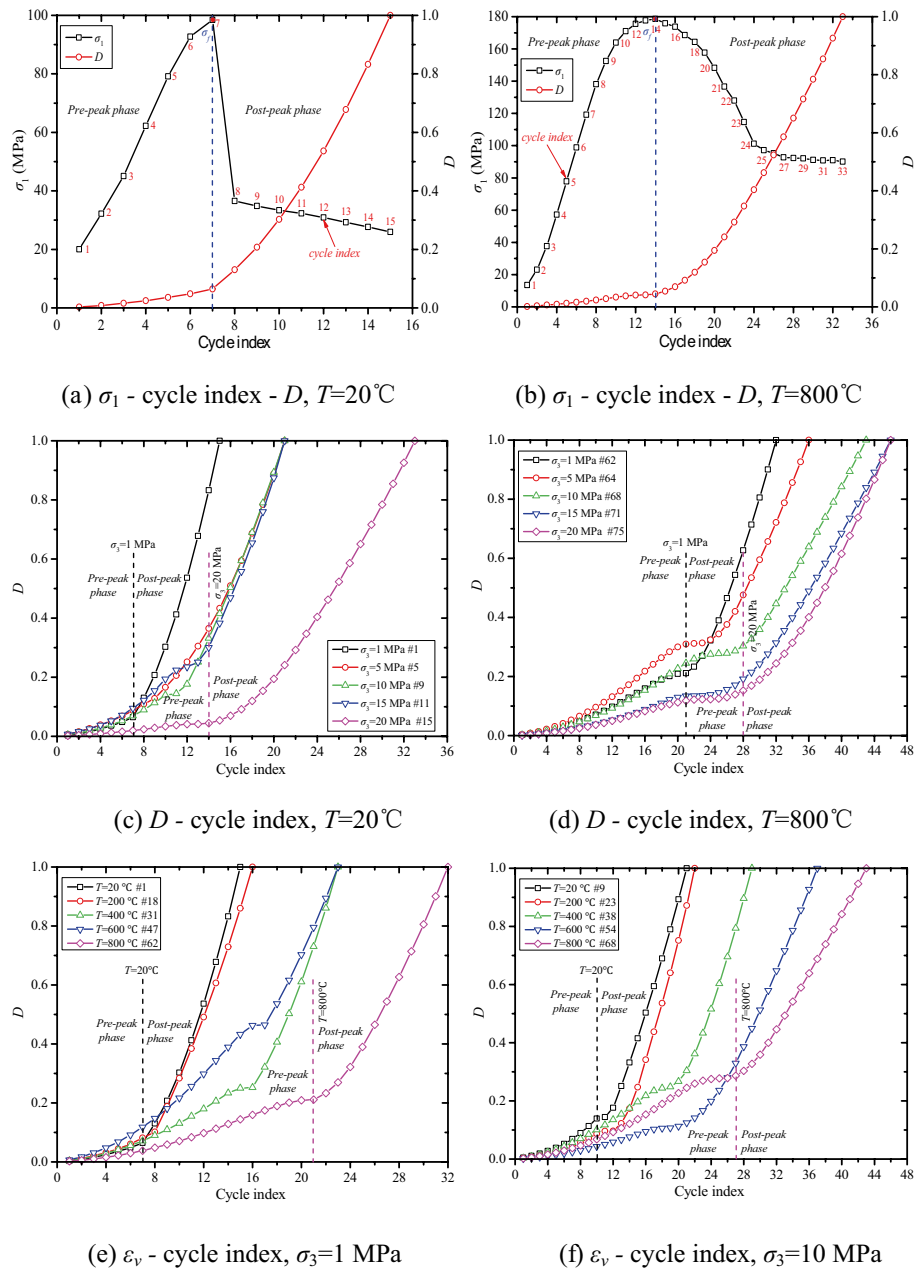


capacity. The post-peak stage reflects the process of the rock sample from the integrity structure to the block structure with the rock sample deformation and development to complete failure after the macroscopic cracks or fracture surfaces appear inside the rock sample. The bearing capacity of rock samples can be maintained by the friction force (residual strength,  $\sigma_r$ ) between the fracture surfaces after failure, The bearing capacity of peak stage, the bearing capacity of rock samples gradually decreases with the increase of cycle index or  $\epsilon_1$ , showing obvious strain-softening phenomenon. Therefore, with the increase of cycle index or  $\epsilon_1$ , the plastic deformation (irreversible deformation) of rock samples continues to

increase from the pre-peak stage to the post-peak stage, which makes the damage accumulated inside the rock samples gradually increase.

2. The evolution process of volumetric strain damage variable ( $D$ ) of the loaded rock samples under different confining pressures and temperatures is basically the same. With the increase of cycle index or axial strain,  $D$  shows a nonlinear increase trend, that is, it increases slowly at the pre-peak stage, and then increases rapidly at the post-peak stage.
3. In the pre-peak stage, with the increase of axial load, the recoverable plastic deformation inside the rock sample gradually increases, which makes the damage degree of

**Fig. 18** Damage variable evolution curve of high-temperature-treated rock sample under confining pressure and temperature



the rock sample gradually increase. With the increase of  $\sigma_3$ , the plastic deformation of rock samples in the pre-peak stage increases continuously, and the  $D_{\text{pre}}$  increases with the increase of  $\sigma_3$ . In the post-peak stage, the high confining pressure can effectively inhibit the slip and expansion deformation of the fracture surface or fracture surface in the rock sample, making  $D_{\text{pos}}$  decrease with the increase of  $\sigma_3$ , and the  $D$  curve of the loaded rock sample slows down, that is, the damage accumulation in the whole process of rock sample deformation to failure shows a slowly increasing trend.

4. With the increase of  $T$ , the downward trend of the stress-strain curve in the post-peak stage is slowed down, and the plastic characteristics of the rock sample are gradually enhanced. The damage accumulation in the whole process of deformation and failure of the rock sample shows a slowly increasing trend, which makes the  $D$  curve of the loaded rock sample slow down. With the increase of  $T$ , the post-peak cycles of rock samples increase significantly, which makes  $D_{\text{pos}}$  increase and  $D_{\text{pre}}$  decrease.

## 5 Conclusions

1. The MTS 815 rock mechanics test system was used to perform triaxial cyclic loading and unloading assays of high-temperature rock samples treated at five different temperatures. With the increase of  $\sigma_3$  and  $T$ , the post-peak stress–strain curve slowly decreased (the stress drop was slower), and the number of hysteresis loops (cycle index) gradually increased. The plastic deformation of the rock sample also gradually increased, and the shape of the stress–strain curve gradually changed from brittle to ductile failure.
2. The strength parameters of the rock sample showed obvious confining pressure enhancement effects and temperature degradation. On one hand, the increase of  $\sigma_3$  and  $T$  increased the degree of damage, but the expansion characteristics showed a delayed phenomenon. On the other hand, as the cycle index increased,  $E_1$  and  $E_u$  increased and then declined, revealing lagging expansion characteristics.  $E_1$  and  $E_u$  simultaneously increased with  $\sigma_3$ , and decreased with increasing  $T$ .
3. The stress-type brittleness index ( $B_s$ ) was established to quantitatively characterize the influence of confining pressure and temperature on the post-peak stress drop state of the rock sample.  $B_s$  increased with the increase of  $N_s$ ,  $B_s$  and  $B_{rs}$  decreased with the increase of  $\sigma_3$ .  $B_s$  also slowly increased with increasing temperature, and  $B_{rs}$  increased rapidly. In addition, with the increase of  $\sigma_3$  and  $T$ , the ductility of the rock sample was enhanced, and the severity of the rock failure decreased. With the increase of cycle index or axial strain, the volumetric strain damage variable ( $D$ ) shows a nonlinear increase trend, that is, it increases slowly at the pre-peak stage, and then increases rapidly at the post-peak stage.

**Acknowledgements** The financial and general supports for this research is supported by the Fundamental Research Funds for the Central Universities (no. 2018XKQYMS07).

## References

- Ai C, Zhang J, Li YW, Zeng J, Yang XL, Wang JG (2016) Estimation criteria for rock brittleness based on energy analysis during the rupturing process. *Rock Mech Rock Eng* 49(12):4681–4698. <https://doi.org/10.1007/s00603-016-1078-x>
- Al-Shayea NA, Khan K, Abduljawwad SN (2000) Effects of confining pressure and temperature on mixed-mode (I-II) fracture toughness of a limestone rock. *Int J Rock Mech Min* 37(4):629–643. [https://doi.org/10.1016/S1365-1609\(00\)00003-4](https://doi.org/10.1016/S1365-1609(00)00003-4)
- Bieniawski ZT (1967) Mechanism of brittle fracture of rock, parts I, II and III. *Int J Rock Mech Min Sci Geomech Abstr* 4(4):395–430. [https://doi.org/10.1016/0148-9062\(67\)90030-7](https://doi.org/10.1016/0148-9062(67)90030-7)
- Chen J, Du C, Jiang DY, Fan JY, He Y (2016) The mechanical properties of rock salt under cyclic loading-unloading experiments. *Geomech Eng* 10(3):325–334. <https://doi.org/10.12989/gae.2016.10.3.325>
- Dwivedi RD, Goel RK, Prasad VVR, Sinha A (2008) Thermo-mechanical properties of Indian and other granites. *Int J Rock Mech Min Sci* 45(3):303–315. <https://doi.org/10.1016/j.ijrmmms.2007.05.008>
- Eberhardta E, Steadb D, Stimpson B (1999) Quantifying progressive pre-peak brittle fracture damage in rock during uniaxial compression. *Int J Rock Mech Min* 36(3):361–380. [https://doi.org/10.1016/S0148-9062\(99\)00019-4](https://doi.org/10.1016/S0148-9062(99)00019-4)
- Fuenkajorn K, Phueakphum D (2010) Effects of cyclic loading on mechanical properties of Maha Sarakham salt. *Eng Geol* 112(1–4):43–52. <https://doi.org/10.1016/j.enggeo.2010.01.002>
- Funatsu T, Seto M, Shimada H (2004) Combined effects of increasing temperature and confining pressure on the fracture toughness of clay bearing rocks. *Int J Rock Mech Min* 41(6):927–938. <https://doi.org/10.1016/j.ijrmmms.2004.02.008>
- Gong FQ, Luo S, Lin G, Li XB (2020) Evaluation of shear strength parameters of rocks by preset angle shear, direct shear and triaxial compression tests. *Rock Mech Rock Eng* 53(5):2505–2519. <https://doi.org/10.1007/s00603-020-02050-1>
- Hajiabdolmajid V, Kaiser P (2003) Brittleness of rock and stability assessment in hard rock tunneling. *Tunn Undergr Space Technol* 18(1):35–48. [https://doi.org/10.1016/S0886-7798\(02\)00100-1](https://doi.org/10.1016/S0886-7798(02)00100-1)
- Heap MJ, Baud P, Meredith PG (2009) Influence of temperature on brittle creep in sandstones. *Geophys Res Lett* 36(19):308–308. <https://doi.org/10.1029/2009GL039373>
- Heuze FE (1983) High-temperature mechanical, physical and thermal properties of granitic rocks: a review. *Int J Rock Mech Min Sci Geomech Abstr* 20(1):3–10. [https://doi.org/10.1016/0148-9062\(83\)91609-1](https://doi.org/10.1016/0148-9062(83)91609-1)
- Hucka V, Das B (1974) Brittleness determination of rocks by different methods. *Int J Rock Mech Min Sci Geomech Abstr* 11(10):389–392. [https://doi.org/10.1016/0148-9062\(74\)91109-7](https://doi.org/10.1016/0148-9062(74)91109-7)
- Jiang CB, Lu TY, Zhang DM, Li GZ, Duan MK, Chen YF, Liu CS (2018) An experimental study of deformation and fracture characteristics of shale with pore–water pressure and under triaxial cyclic loading. *R Soc Open Sci* 5(8):180670. <https://doi.org/10.1098/rsos.180670>
- Just J, Kontny A (2012) Thermally induced alterations of minerals during measurements of the temperature dependence of magnetic susceptibility: a case study from the hydrothermally altered Soultz-Sous-Forêts granite. *France Int J Earth Sci* 101(3):819–839. <https://doi.org/10.1007/s00531-011-0668-9>
- Labuz JF, Zang A (2012) Mohr–Coulomb failure criterion. *Rock Mech Rock Eng* 45(6):975–979. <https://doi.org/10.1007/s00603-012-0281-7>
- Lee YK, Pietruszczak S, Choi BH (2012) Failure criteria for rocks based on smooth approximations to Mohr–Coulomb and Hoek–Brown failure functions. *Int J Rock Mech Min* 56(12):146–160. <https://doi.org/10.1016/j.ijrmmms.2012.07.032>
- Li YY, Zhang SC, Zhang BL (2018) Dilatation characteristics of the coals with outburst proneness under cyclic loading conditions and the relevant applications. *Geomech Eng* 14(5):459–466. <https://doi.org/10.12989/gae.2018.14.5.459>
- Li M, Wang DM, Shao ZL (2020a) Experimental study on changes of pore structure and mechanical properties of sandstone after high - temperature treatment using nuclear magnetic resonance. *Eng Geol* 275:105739. <https://doi.org/10.1016/j.enggeo.2020.105739>
- Li YW, Zhao YD, Tang JZ, Zhang LY, Zhou YY, Zhu XY, Jia D, Chen M (2020b) Rock damage evolution model of pulsating fracturing based on energy evolution theory. *Energy Sci Eng* 8(4):1050–1067. <https://doi.org/10.1002/ese3.567>
- Liu XS, Ning JG, Tan YL, Gu QH (2016) Damage constitutive model based on energy dissipation for intact rock subjected to cyclic loading. *Int J Rock Mech Min* 85(5):27–32. <https://doi.org/10.1016/j.ijrmmms.2016.03.003>

- Mahanta B, Singh TN, Ranjith PG (2016) Influence of thermal treatment on mode I fracture toughness of certain Indian rocks. *Eng Geol* 210:103–114. <https://doi.org/10.1016/j.enggeo.2016.06.008>
- Martin CD, Chandler NA (1994) The progressive fracture of Lac du bonnet granite. *Int J Rock Mech Min Sci Geomech Abstr* 31(6):643–659. [https://doi.org/10.1016/0148-9062\(94\)90005-1](https://doi.org/10.1016/0148-9062(94)90005-1)
- Masri M, Sibai M, Shao JF, Mainguy M (2014) Experimental investigation of the effect of temperature on the mechanical behavior of Tournemire shale. *Int J Rock Mech Min* 70:185–191. <https://doi.org/10.1016/j.ijrmms.2014.05.007>
- Meng QB, Zhang MW, Han LJ, Pu H, Nie TY (2016) Effects of acoustic emission and energy evolution of rock specimens under the uniaxial cyclic loading and unloading compression. *Rock Mech Rock Eng* 49(10):3873–3886. <https://doi.org/10.1007/s00603-016-1077-y>
- Meng LB, Li TB, Cai GJ (2017) Temperature effects on the mechanical properties of slates in triaxial compression test. *J Mt Sci Engl* 14(12):2581–2588. <https://doi.org/10.1007/s11629-016-4171-4>
- Meng QB, Zhang MW, Han LJ, Pu H, Chen YL (2018) Acoustic emission characteristics of red sandstone specimens under uniaxial cyclic loading and unloading compression. *Rock Mech Rock Eng* 51(4):969–988. <https://doi.org/10.1007/s00603-017-1389-6>
- Meng QB, Qian W, Liu JF, Zhang MW, Lu MM, Wu Y (2020a) Analysis of triaxial compression deformation and strength characteristics of limestone after high temperature. *Arab J Geosci* 13(4):153. <https://doi.org/10.1007/s12517-020-5151-0>
- Meng QB, Wang CK, Liu JF, Zhang MW, Lu MM, Wu Y (2020b) Physical and micro-structural characteristics of limestone after high temperature exposure. *Bull Eng Geol Environ* 79(3):1259–1274. <https://doi.org/10.1007/s10064-019-01620-0>
- Meng QB, Liu JF, Ren L, Pu H, Chen YL (2021) Experimental study on rock strength and deformation characteristics under triaxial cyclic loading and unloading conditions. *Rock Mech Rock Eng* 54(2):777–797. <https://doi.org/10.1007/s00603-020-02289-8>
- Mogi K (1972) Effect of the triaxial stress system on fracture and flow of rocks. *Phys Earth Planet Interiors* 5:318–324. [https://doi.org/10.1016/0031-9201\(72\)90102-1](https://doi.org/10.1016/0031-9201(72)90102-1)
- Molen IVD (1981) The shift of the  $\alpha$ - $\beta$  transition temperature of quartz associated with the thermal expansion of granite at high pressure. *Tectonophysics* 73(4):323–342. [https://doi.org/10.1016/0040-1951\(81\)90221-3](https://doi.org/10.1016/0040-1951(81)90221-3)
- Nygård R, Gutierrez M, Bratli RK, Høeg K (2006) Brittle–ductile transition, shear failure and leakage in shales and mudrocks. *Mar Pet Geol* 23(2):201–212. <https://doi.org/10.1016/j.marpetgeo.2005.10.001>
- Pei F, Ji HG, Zhang TZ (2019) Energy evolution and mechanical features of granite subjected to triaxial loading - unloading cycles. *Adv Civ Eng* 2:1–11. <https://doi.org/10.1155/2019/9871424>
- Ranjith PG, Viete DR, Chen BJ, Perera MSA (2012) Transformation plasticity and the effect of temperature on the mechanical behavior of Hawkesbury sandstone at atmospheric pressure. *Eng Geol* 151(29):120–127. <https://doi.org/10.1016/j.enggeo.2012.09.007>
- Rao MVMS, Ramana YV (1992) A study of progressive failure of rock under cyclic loading by ultrasonic and AE monitoring techniques. *Rock Mech Rock Eng* 25(4):237–251. [https://doi.org/10.1016/0148-9062\(93\)90049-J](https://doi.org/10.1016/0148-9062(93)90049-J)
- Ray SK, Sarkar M, Singh TN (1999) Effect of cyclic loading and strain rate on the mechanical behaviour of sandstone. *Int J Rock Mech Min* 36(4):543–549. [https://doi.org/10.1016/S0148-9062\(99\)00016-9](https://doi.org/10.1016/S0148-9062(99)00016-9)
- Renani HR, Martin CD (2020) Slope stability analysis using equivalent Mohr–Coulomb and Hoek–Brown criteria. *Rock Mech Rock Eng* 53(1):13–21. <https://doi.org/10.1007/s00603-019-01889-3>
- Sha S, Rong G, Tan J, He RH, Li BW (2020) Tensile strength and brittleness of sandstone and granite after high-temperature treatment: a review. *Arab J Geosci* 13(14):598. <https://doi.org/10.1007/s12517-020-05647-6>
- Shen YJ, Hou X, Yuan JQ, Wang SF, Zhao CH (2020) Thermal cracking characteristics of high-temperature granite suffering from different cooling shocks. *Int J Fract* 225(2):153–168. <https://doi.org/10.1007/s10704-020-00470-2>
- Shkuratnik VL, Kravchenko OS, Filimonov YL (2019) Stresses and temperature affecting acoustic emission and rheological characteristics of rock salt. *J Min Sci* 55(4):531–537. <https://doi.org/10.1134/S1062739119045879>
- Su HJ, Jing HW, Yin Q, Yu LY, Wang YC, Wu XJ (2017) Strength and deformation behaviors of veined marble specimens after vacuum heat treatment under conventional triaxial compression. *Acta Mech Sin Pra* 33(5):886–898. <https://doi.org/10.1007/s10409-017-0653-z>
- Sun Q, Zhang WQ, Xue L, Zhang ZZ, Su TM (2015) Thermal damage pattern and thresholds of granite. *Environ Earth Sci* 74(3):2341–2349. <https://doi.org/10.1007/s12665-015-4234-9>
- Sun Q, Zhang WQ, Su T, Zhu S (2016) Variation of wave velocity and porosity of sandstone after high temperature heating. *Acta Geophys* 64(3):633–648. <https://doi.org/10.1515/acgeo-2016-0021>
- Tian H, Kempka T, Xu NX, Ziegler M (2012) Physical properties of sandstones after high temperature treatment. *Rock Mech Rock Eng* 45(6):1113–1117. <https://doi.org/10.1007/s00603-012-0228-z>
- Wang HL, Xu WY, Cai M, Xiang ZP, Kong Q (2017) Gas permeability and porosity evolution of a porous sandstone under repeated loading and unloading conditions. *Rock Mech Rock Eng* 50(8):2071–2083. <https://doi.org/10.1007/s00603-017-1215-1>
- Wang P, Yin TB, Liang DX, Li XB, Zhang SS, Bai L (2019) Dynamic properties of thermally treated granite subjected to cyclic impact loading. *Rock Mech Rock Eng* 52(4):991–1010. <https://doi.org/10.1007/s00603-018-1606-y>
- Wei SJ, Yang YS, Su CD, Cardoso SR, Wang H (2019) Experimental study of the effect of high temperature on the mechanical properties of coarse sandstone. *Appl Sci Basel* 9(12):2424. <https://doi.org/10.3390/app9122424>
- Wong TF, Baud P (2012) The brittle–ductile transition in porous rock: a review. *J Struct Geol* 44:25–53. <https://doi.org/10.1016/j.jsg.2012.07.010>
- Wong TF, David C, Zhu W (1997) The transition from brittle faulting to cataclastic flow in porous sandstones: mechanical deformation. *J Geophys Res* 102(2):3009–3026. <https://doi.org/10.1029/96JB03281>
- Xiao F, Jiang DY, Wu F, Zou QL, Chen J, Chen B, Sun ZG (2020a) Effects of prior cyclic loading damage on failure characteristics of sandstone under true-triaxial unloading conditions. *Int J Rock Mech Min* 132(8):104379. <https://doi.org/10.1016/j.ijrmms.2020.104379>
- Xiao WJ, Zhang DM, Yang H, Li XM, Ye ML, Li SJ (2020b) Laboratory investigation of the temperature influence on the mechanical properties and fracture crack distribution of rock under uniaxial compression test. *Bull Eng Geol Environ* 80(2):1585–1598. <https://doi.org/10.1007/s10064-020-01993-7>
- Yang SQ, Hu B (2018) Creep and long-term permeability of a red sandstone subjected to cyclic loading after thermal treatments. *Rock Mech Rock Eng* 51(10):2981–3004. <https://doi.org/10.1007/s00603-018-1528-8>
- Yang SQ, Jing HW, Wang SY (2012) Experimental investigation on the strength, deformability, failure behavior and acoustic emission locations of red sandstone under triaxial compression. *Rock Mech Rock Eng* 45(4):583–606. <https://doi.org/10.1007/s00603-011-0208-8>
- Yang SQ, Ranjith PG, Jing HW, Tian WL, Ju Y (2017) An experimental investigation on thermal damage and failure mechanical behavior of granite after exposure to different high temperature

- treatments. *Geothermics* 65:180–197. <https://doi.org/10.1016/j.geothermics.2016.09.008>
- Zhang JC, Zhou SH, Fang LG, Fan JY, Xu XH (2013) Effects of axial cyclic loading at constant confining pressures on deformational characteristics of anisotropic argillite. *J Cent South Univ* 20(3):799–811. <https://doi.org/10.1007/s11771-013-1551-6>
- Zhang LY, Mao XB, Li M, Li B, Liu RX, Lu AH (2020) Brittle–ductile transition of mudstone in coal measure rock strata under high temperature. *Int J Geomech* 20(1):04019149. [https://doi.org/10.1061/\(ASCE\)GM.1943-5622.0001549](https://doi.org/10.1061/(ASCE)GM.1943-5622.0001549)
- Zhao XG, Cai M, Wang J, Ma LK (2013) Damage stress and acoustic emission characteristics of the Beishan granite. *Int J Rock Mech Min* 64:258–269. <https://doi.org/10.1016/j.ijrmms.2013.09.003>
- Zhao GM, Wang C, Liang DX (2018a) Comparative experimental studies of acoustic emission characteristics of sandstone and mudstone under the impacts of cyclic loading and unloading. *Int J Distrib Sens N* 14(8):1550147718795552. <https://doi.org/10.1177/1550147718795552>
- Zhao J, Feng XT, Zhang XW, Zhang Y ZYY, Yang CX (2018b) Brittle–ductile transition and failure mechanism of Jinping marble under true triaxial compression. *Eng Geol* 232:160–170. <https://doi.org/10.1016/j.enggeo.2017.11.008>

**Publisher's Note** Springer Nature remains neutral with regard to jurisdictional claims in published maps and institutional affiliations.